Anonymous Referee #1 Received and published: 21 October 2020

General comments: The interaction between aerosols and the boundary layer is a hot topic in the study of the formation mechanism of air pollution in polluted areas. The aim of this paper is to evaluate the fundamental interaction between PM and ABL structure and to further quantitatively estimate the effect of aerosol radiative forcing (ARF) on ABL structure. The paper addressed relevant scientific questions and presented novel concepts, ideas and tools. The scientific methods and assumptions were almost valid and clearly outlined so that substantial conclusions were reached. The description of experiments and calculations were almost complete and precise to allow their reproduction by fellow scientists except some points. I think the manuscript could be considered to be accepted after major revision.

Response: Thank the reviewer for the encouragements and constructive suggestions. According to the reviewer's suggestions, we have done our best to revise our manuscript. The modifications have been highlighted in red in the following marked-up manuscript version.

Major comments:

1. Seven cases spanning two months were selected in the paper to discuss the threshold value of aerosol radiative forcing's effect on the contaminated areas' boundary layer structure. Are these cases representative, and would the thresholds change in other cases?

Response: Thank the reviewer for the comments. Firstly, this campaign was launched in Beijing city to obtain the vertical profile observations of meteorological elements in the boundary layer. This experiment lasted from November 2018 to January 2019, and we obtained two-month data sets that can reflect the atmospheric boundary layer structure and atmospheric pollution in winter in Beijing. Second, we need to restate that the threshold value of aerosol radiative forcing's effect on the boundary layer structure was obtained based on the whole two-month data rather than the several cases. Only in the qualitative analysis of the relationship between the aerosol radiation effect and the boundary layer we selected cases to analyze and explain. It means the Figs. 4-7 involved in the quantitative analysis of aerosol radiative forcing influences on the boundary layer structure were processed and obtained based on the whole two-month datasets. We think the threshold value results could be representative and reflect specific effects of aerosol radiation forcing on boundary layer structure in winter in Beijing.

2. With only a finite number of points in Fig. 4, does the current fitting relationship pass the significance test?

Response: Thank the reviewer for the comments and suggestions. We need to explain that the current fitting relationships in Fig. 4 have passed the significant test. More details were shown below:

We used SPSS V19.0 software to calculate the relationship coefficients between $PM_{2.5}$

and TOA, ATM, SFC, and |SFC-ATM|, respectively, shown in Table 1. The significance levels between $PM_{2.5}$ and TOA, SFC, and |SFC-ATM| are respectively less than 0.01, indicating that they have passed the 99% significance test and have a significant correlation, respectively. The significance level between $PM_{2.5}$ and ATM is 0.021, grater than 0.01 and less than 0.05, indicating that they have passed the 95% significance test and have a reasonable correlation.

Table 1. Relationship test

		N	Relationship coefficient (R^2)	Significance level
a	$PM_{2.5}$ & TOA	13	0.75	0.000
b	$PM_{2.5}$ & ATM	13	0.40	0.021
c	$PM_{2.5}$ & SFC	13	0.83	0.000
d	$PM_{2.5}$ & |SFC-ATM|	13	0.81	0.000

3. In Fig. 1b, the results for aerosol radiative forcing have values only for individual moments of the day, and a detailed explanation of how they relate to hourly variations in atmospheric conditions and PM concentrations is needed.

Response: Thank the reviewer for the constructive suggestions. According to the reviewer's suggestions, we have added a detailed explanation of how the aerosol radiative forcing relates to hourly variations in atmospheric conditions and PM concentrations in the revised manuscript.

4. What is the physical mechanism by which |SFC-ATM| affects the threshold of atmospheric stability?

Response: Thank the reviewer for the comments. |SFC-ATM|, defined as the absolute value of the difference between SFC and ATM, represents aerosols' combined action on the solar radiation reaching the aerosol layer and the ground. Larger values of |SFC-ATM| indicate either stronger aerosol scattering (higher SFC) or absorption effects (higher ATM), or indicate both stronger aerosol scattering and absorption effects. No matter which one causes the increased |SFC-ATM|, they all imply a more significant temperature difference between the surface and the above atmosphere layer. That means a higher |SFC-ATM| would lead to a more stable atmospheric stratification, which would suppress the turbulence development.

5. When calculating TKE, why a one-hour wind standard deviation was chosen rather than a half-hour or two-hour standard deviation? In lines 141-152, the temporal and spatial scales of TKE need to be clarified.

Response: Thank the reviewer for the comments and suggestions. Considering the time series of the boundary layer meteorological elements profile were displayed on the hourly scale, we choose to calculate one-hour TKE for better analyze the relationship among them. Regarding the temporal and spatial scales of TKE have been added in the

calculation part of Section 2.

6. Fig. 1 is of low quality and should be improved. In Fig. 1-(a)-III, why does the PM not increase with decreasing ABLH?

Response: Thank the reviewer for the comments and suggestions, and we have improved the quality of Fig.1. In Fig.1-(a)-III, $PM_{2.5}$ concentrations were generally below ~40 μg m^{-3}, when there was a decreasing ABLH, the $PM_{2.5}$ concentrations have slightly increased. The $PM_{2.5}$ concentrations did not increase as significantly as those in heavy pollution phases of cases I and II. Due to the drop of vertical diffusion height, the PM was accumulated at the ground level, increasing the surface PM concentrations to some degree. However, during the clean period III, Beijing was controlled by clean and dry winds, the air humidity was quite low. With less PM loading and low humidity near the surface, the heterogeneous reaction was not intense. The weak secondary aerosol formation would not lead to an outbreak of PM concentrations near the surface. That is the reason that the PM did not increase much with decreasing ABLH.

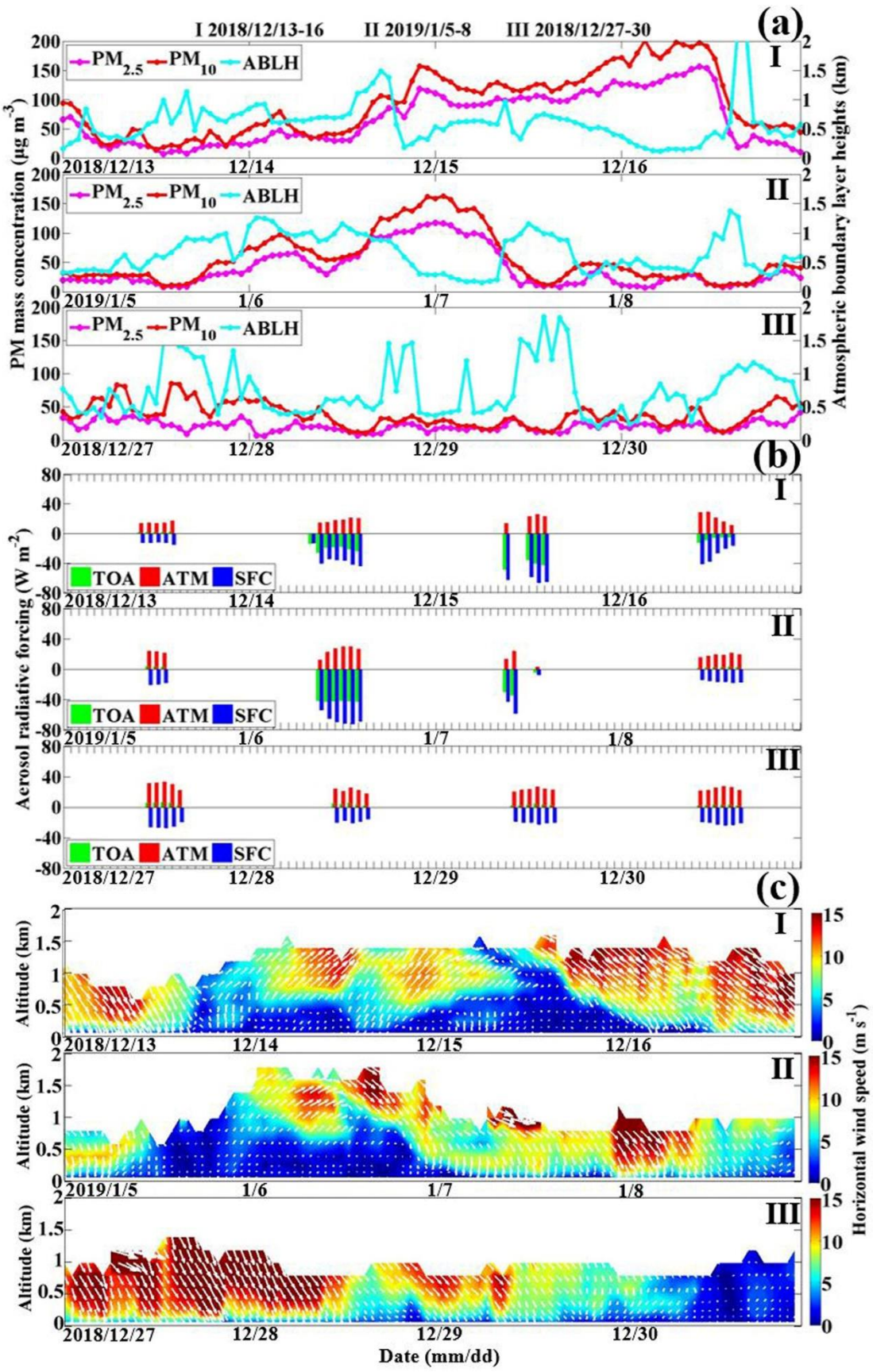

Figure 1. Temporal evolution of (a) the PM mass concentration and atmospheric boundary layer height ($PM_{2.5}$: solid pink lines; PM_{10}: solid red lines; ABLH: solid blue

lines), (b) aerosol radiative forcing at the top (TOA; green bars), surface (SFC; blue bars) and interior of the atmospheric column (ATM; red bars), and (c) horizontal wind vector profiles (shaded colors: wind speeds; white arrows: wind vectors) during the typical haze pollution episodes of I (2018/12/13-16) and II (2019/1/5-8) as well as the typical clean period of III (2018/12/27-30).

7. In Figure 1-(b) I and II, the TOA varied significantly. What is the reason?

Response: Thank the reviewer for the comments and suggestions. As shown in Fig. 4, TOA forcing was proportional to the $PM_{2.5}$ concentration. With the increase in $PM_{2.5}$ concentration, elevated aerosol loading near the surface would scatter more solar radiation back into outer space and cause less solar radiation reaching the ground, corresponding to a cooling of the surface and making negative SFC. TOA means the aerosol radiative forcing at the top of the atmosphere column and is the sum of ATM and SFC. Considering that anthropogenic aerosols are mostly scattering aerosols, the SFC forcing is generally stronger than ATM, corresponding to a cooling of the earth-atmosphere system. The TOA forcing was thus usually negative and had a similar trend with SFC. Thus, in Figure 1-(b) I and II, with PM concentrations increasing, the TOA varied significantly.

8. There are very interesting results for PM and temperature in Figure 2. What are the diurnal characteristics of the potential temperature? Does potential temperature affect the diurnal concentration of $PM_{2.5}$?

Response: Thank the reviewer for the comments and suggestions. Figure 2 shows temporal variations in the vertical profiles of (a) the virtual potential temperature gradient ($\partial\theta v/\partial z$), (b) pseudoequivalent potential temperature gradient ($\partial\theta se/\partial z$) and (c) temperature inversion phenomenon (shaded colors: inversion intensity) during the typical haze pollution episodes of I (2018/12/13-16) and II (2019/1/5-8) as well as the typical clean period of III (2018/12/27-30). Figures 2(c) have shown the relationship between PM and temperature structure. For example, when the temperature vertical gradient is positive means a temperature inversion occurs. This abnormal temperature structure would lead to a stable stratification with a positive potential temperature gradient. Figure 2(a)-(b) exactly present the potential temperature conditions corresponding to the temperature structure in Fig. 2(c). The temporal variations in the vertical profiles of (a) the virtual potential temperature gradient ($\partial\theta v/\partial z$) and (b) pseudoequivalent potential temperature gradient ($\partial\theta se/\partial z$) can represent a diurnal variation in potential temperature (stratification stability) which influence the diurnal change in $PM_{2.5}$. The specific analysis was provided in section 3.2.

9. In Figure 4, other dots represent mean data. How is it calculated?

Response: Thank the reviewer for the comments. In Fig. 4, the other dots represent mean data calculated by averaging the daily data at a fixed step length. The daily data means daily mean values of TOA, ATM, SFC, and corresponding daily averaged $PM_{2.5}$ mass concentration from 27 November 2018 to 25 January 2019 in Beijing. The mean

$PM_{2.5}$ concentrations were obtained by averaging daily $PM_{2.5}$ concentrations at intervals of 10 μg m^{-3}. The mean TOA, ATM, and SFC were obtained after the corresponding daily TOA, ATM, and SFC average, respectively. For example, all daily $PM_{2.5}$ concentrations greater than 40 μg m^{-3} and less than 50 μg m^{-3} were averaged as a mean $PM_{2.5}$ concentration, and TOA values (ATM; SFC) corresponding to this daily $PM_{2.5}$ concentration range were also averaged as a mean TOA (ATM; SFC). We have added a more detailed calculation description in the Fig. 4 caption.

10. The empirical relationships of TKE and |SFC-ATM| are very interesting in Figure 6 (left upper panel). It established the thermodynamic relationship between ARF and TKE by using the measured data. Why does the fitting relationship fit so well below 300 meters?

Response: Thank the reviewer for the comments. As we can see in Fig. 6, the exponential relationship between TKE and |SFC-ATM| was notable in the lower layers (below ~300 m) and gradually deteriorated with the increasing altitude. We all know that aerosols are mainly concentrated in the lower atmosphere, contributing the most to the SFC and ATM forcing. The stratification stability induced by the aerosol radiative effect would mainly occur in lower layers. The much better exponential relationship between TKE and |SFC-ATM| in the lower layers exactly further confirmed that the considerable change in atmospheric stratification caused by aerosols indeed existed and was mainly shown in the lower layers. With the increase of altitude, aerosol loading is in decline; thus, aerosol radiative effect on the atmospheric stability drops. Furthermore, at a relatively high altitude, the aerosol is few, and the radiation effect has almost no influence on the stability of the atmosphere layer.

11. The ARF threshold is about 55 W m^{-2}. What about the concentration of $PM_{2.5}$? Is it possible to derive a threshold concentration for $PM_{2.5}$ based on current observational relationships. The $PM_{2.5}$ threshold would be a very meaningful target for air pollution control.

Response: Thank the reviewer for the comments and constructive suggestions. As we can see from Fig. 4(d), the exponential relationship between $PM_{2.5}$ and |SFC-ATM| was founded. According to the linear fitting equation of $y=0.49x+31.21$ (x: $PM_{2.5}$; y: |SFC-ATM|), it is possible to derive a threshold concentration for $PM_{2.5}$ based on the current |SFC-ATM| threshold of about 55 W m^{-2}.

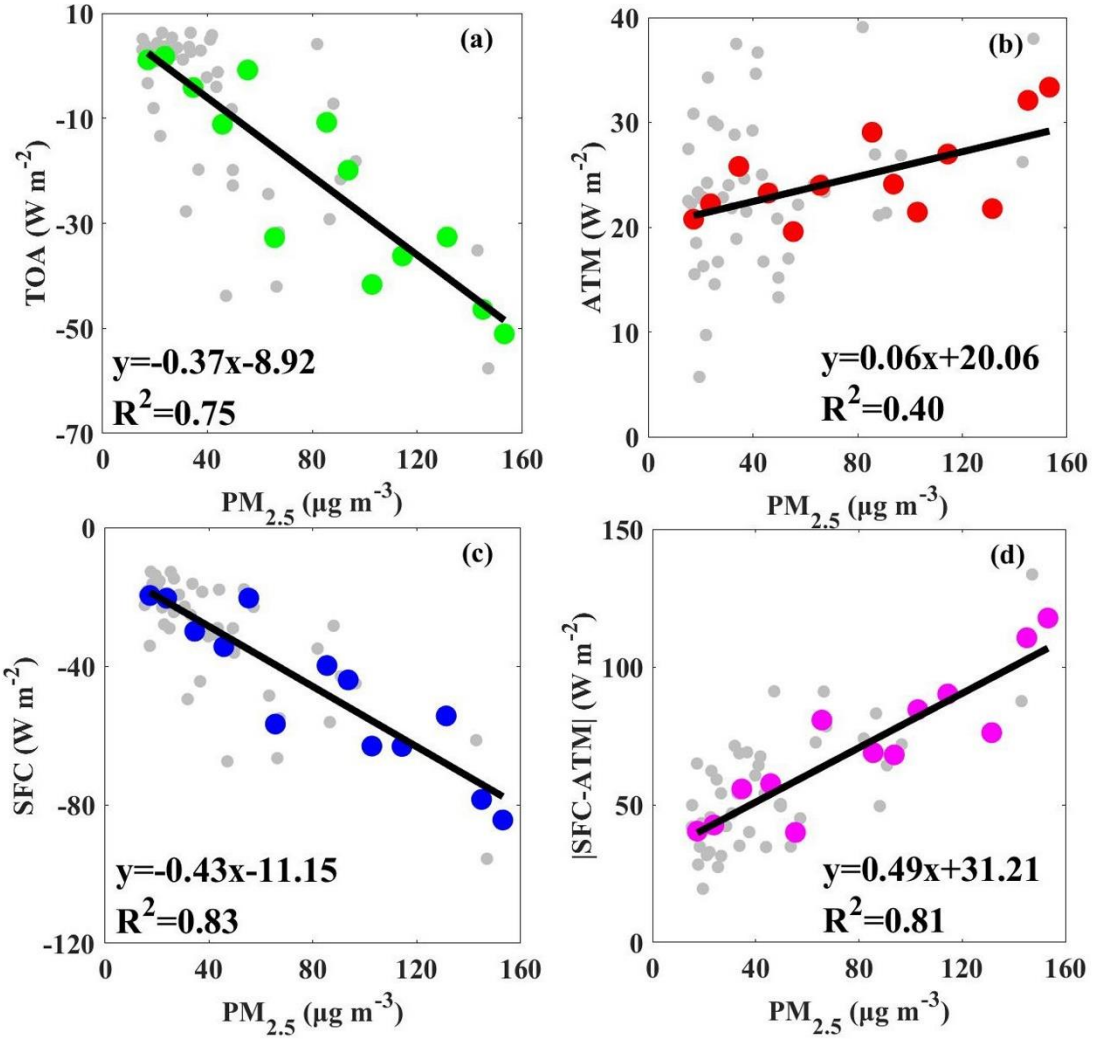

Figure 4. Scatter plots of the $PM_{2.5}$ mass concentration (x) versus aerosol radiative forcing at the surface (SFC; y; a), interior of the atmospheric column (ATM; y; b) and top of the atmospheric column (TOA; y; c) as well as the absolute difference of SFC and ATM (|SFC-ATM|; y; d), respectively (gray dots: daily data; other dots: mean data). (The daily data means daily mean values of TOA, ATM, SFC, and corresponding daily averaged $PM_{2.5}$ mass concentration from 27 November 2018 to 25 January 2019 in Beijing. The mean $PM_{2.5}$ concentrations were obtained by averaging daily $PM_{2.5}$ concentrations at intervals of 10 μg m^{-3}. The mean TOA, ATM, and SFC were obtained after the corresponding daily TOA, ATM, and SFC average, respectively. For example, all daily $PM_{2.5}$ concentrations greater than 40 μg m^{-3} and less than 50 μg m^{-3} were averaged as a mean $PM_{2.5}$ concentration, and TOA values (ATM; SFC) corresponding to this daily $PM_{2.5}$ concentration range were also averaged as a mean TOA (ATM; SFC)).

12. The review of aerosol radiative forcing in the introduction needs to be strengthened.

Response: Thank the reviewer for the comments and constructive suggestions. As the reviewer's suggested, the review of aerosol radiative forcing in the introduction has been strengthened.

13. Conclusion needs to be subdivided and further simplified.

Response: Thank the reviewer for the comments and constructive suggestions. As you suggested, the Conclusion has been subdivided and further simplified.

14. In Figure 8, TKE >2 m^2 s^{-2}, |SFC-ATM| ~55 W m^{-2}. Are these thresholds generalizable?

Response: Thank the reviewer for the comments. Firstly, this campaign was launched in Beijing city to obtain the vertical profile observations of meteorological elements in the boundary layer. This experiment lasted from November 2018 to January 2019, and we obtained two-month data sets that can reflect the atmospheric boundary layer structure and atmospheric pollution in winter in Beijing. Second, the threshold value of aerosol radiative forcing's effect on the boundary layer structure was obtained based on the whole two-month data. It means Fig. 8 involved in the quantitative analysis of aerosol radiative forcing influences on the boundary layer structure were processed and obtained based on the whole two-month datasets. We think the threshold value results could be representative and reflect specific effects of aerosol radiation forcing on boundary layer structure in winter in Beijing.

Minor comments:

English writing should be polished. Some sentences were hard to read.

1. e.g. line 18-20 “Multi-episode contrastive analysis stated the key to determining whether haze outbreak or dissipation was the ABL structure (i.e., stability and turbulence kinetic energy (TKE)) satisfied relevant conditions.” Should be “Multi-period comparative analysis indicated that the key to determining whether the haze outbreak or dissipation occurs is whether the ABL structure (i.e., stability and turbulent kinetic energy (TKE)) satisfies the relevant conditions.”

Response: Thank the reviewer very much for this gramma suggestion. We have corrected it.

2. Line 22-23. “SFC and ATM is respectively the ARF at the surface and interior of the atmospheric column” should be “SFC and ATM are the ARFs at the surface and interior of the atmospheric column, respectively.”

Response: Thank the reviewer very much for this gramma suggestion. We have corrected it.

3. Line 37-38. (Li et al., 2020; Xu et al., 2019), should be cited at the end of this sentence.

Response: Thank the reviewer for this suggestion. We have corrected it.

4. Line 316 two “dropped to”.

Response: Thank the reviewer for pointing out this mistake. We have corrected it.

Anonymous Referee #2 Received and published: 14 November 2020

1. The authors attempted to propose a parameter, $|SFC-ATM|$ for quantification of the impact of aerosol radiative forcing (ARF) on the atmospheric boundary layer (ABL) structure. Why did the author use the ARF of the interior of the atmosphere column (ATM) rather than the ARF in the ABL since most of aerosols or particulate matters are trapped in the atmospheric boundary layer?

Response: Thanks for the reviewer's comment. First of all, when quantifying the impact of aerosols on climate change, it is more to judge its impact on the earth-atmosphere system as a whole, so the top of the atmosphere's choice will be more reasonable. Secondly, in our previous work, we used the path radiation in MODIS data as a key parameter for calculating the atmospheric SSA, which represents the radiation value at the top of the atmosphere (TOA). In order to facilitate the comparison and verification in the later calculation process, we chose the same height to calculate the relevant radiation results, which can perform unified calculation and analysis both on the top of the atmosphere. We believe this can get more representative results in aerosol radiation research (Gong et al., 2014; Lee et al., 2007; Xin et al., 2016). Finally, as the reviewer said, aerosols are concentrated in the boundary layer and few in the stratosphere. It is because most aerosols exist in the boundary layer that we have verified in the previous sensitivity test, and the calculations at the top of the boundary layer and the top of the atmosphere are as follows:

$$\Delta F^{AEROSOL} = (\Delta F_{aero}^{TOA} - \Delta F_{non-aero}^{TOA}) - (\Delta F_{aero}^{SFC} - \Delta F_{non-aero}^{SFC}) \quad (1)$$

$$\Delta F = F^{\text{downward}} - F^{\text{upward}} \quad (2)$$

Where ΔF denotes the net downward flux (downward minus upward radiation); the subscripts "TOA" and "SFC" denote the top of the atmosphere/boundary layer and the surface; and “aero” and “non-aero” denote dusty and clean skies (Chou et al., 2002). Since there are few aerosols at high altitudes, the ΔF aero- ΔF non-aero itself is derived from the boundary layer difference. The ΔF aero- ΔF non-aero at high altitudes is negligible. So the radiative forcing generated by aerosols will not be significantly different because of the ABL or the top of the atmosphere. For these three reasons, we finally chose the top of the atmosphere for analysis.

Chou, M., Chan, P., and Wang, M.: Aerosol radiative forcing derived from SeaWiFS-retrieved aerosol optical properties, J. Atmos. Sci., 59, 748–757, http://dx.doi.org/10.1175/1520-0469(2002), 2002.

Gong, C., Xin, J., Wang, S., Wang, Y., Wang, P., Wang, L., and Li, P.: The aerosol direct radiative forcing over the Beijing metropolitan area from 2004 to 2011, J. Aerosol Sci., 69, 62-70, https://doi.org/10.1016/j.jaerosci.2013.12.007, 2014.

Xin, J., Gong, C., Wang, S., and Wang, Y.: Aerosol direct radiative forcing in desert and semi-desert regions of northwestern China, Atmos. Res., 171, 56-65, https://doi.org/10.1016/j.atmosres.2015.12.004, 2016.

Lee K., Li Z., Wong M., Xin J., Wang Y., Hao W., and Zhao F.: Aerosol single scattering albedo estimated across China from a combination of ground and satellite measurements, J. Geophys. Res.: Atmos., 112(D22), https://doi.org/10.1029/2007JD009077, 2007.

2. Impact of ARF on reduction of surface-reaching shortwave radiation and heating/cooling of the atmosphere is dependent on not only aerosol loadings in the atmosphere (e.g., AOD) but also aerosol optical or radiative properties such as single-scattering albedo (SSA). What value(s) of SSA was (were) used in the numerical simulations with the SBDART radiation transfer model and how the threshold value changes single-scattering albedo (SSA)? It will be helpful if the author may provide more details about the configurations and inputs utilized in the simulations.

Response: Thanks for the reviewer's comment. We have added relative details in the manuscript after the first referee round. "The algorithm of SBDART (Santa Barbara DISORT Atmospheric Radiative Transfer) (Levy et al., 2007) is the core model to calculate the radiative forcing parameters. A standard mid-latitude atmosphere is used in SBDART in Beijing. AOD and Angstrom Exponent (AE) at 550 nm were obtained from sun-photometer. Multiple sets of Single Scattering Albedo (SSA) and backscattering coefficient were calculated based on MIE theory, and surface albedo & path radiation were read from MODIS (MOD04), which is used to calculate radiative forcing at the top of atmosphere (TOA). The TOA results were combined with MODIS observations, the result which has the lowest deviation is defined as the actual parameters of aerosols, and this set of parameters would be used to calculate the radiative forcing at the surface, top, and interior of the atmospheric column (Gong et al., 2014). Hourly radiative forcing parameters, including the ARF at the top (TOA), surface (SFC), and interior of the atmospheric column (ATM) at an observation site in Beijing can be calculated based on this algorithm. More detailed descriptions are provided in our previous work (Gong et al., 2014; Xin et al., 2016)." was added in Section 2.

3. Is it necessary to use both virtual potential temperature gradient and pseudoequivalent potential temperature gradient to define the atmospheric stability since both have very similar time-height cross section distribution patterns? Please provide a description on how to use these two gradients to define the atmospheric stability and what are the advantages of using these two gradients rather than potential temperature gradient in determining the atmospheric stability?

Response: Thank the reviewer very much for this comment. Using both virtual potential temperature gradient and pseudoequivalent potential temperature gradient to define the atmospheric stability is more accurate and closer to the real atmosphere condition. Because the real atmosphere consists of saturated and unsaturated air masses. The negative virtual potential temperature gradient means absolute unstable stratifications for both saturated and unsaturated air masses, rare except in the lower layers where it is possible. When the virtual potential temperature gradient is positive while the

pseudoequivalent potential temperature gradient is negative means a stratification of conditional instability. The atmosphere stratification is unstable for a saturated air mass and stable for an unsaturated air mass. The stratification of conditional instability will become unstable once the saturated air mass reaches the condensation height due to strong local convection or substantial uplift of dynamic factors. The positive pseudoequivalent potential temperature gradient means absolute stable stratifications for both saturated and unsaturated air masses. However, the potential temperature gradient in determining the atmospheric stability only refers to unsaturated air masses. These are the reason that we choose to use both virtual potential temperature gradient and pseudoequivalent potential temperature gradient to define the atmospheric stability.

4. Figs. 2-3: It is suggested to replot these figures by including specific months and dates in x-axis for a better view. In addition, right y-axis should be $PM_{2.5}$ rather than PM for both figures. Please correct them.

Response: Thank the reviewer very much for this comment and suggestion. As you suggested, we have replotted Fig. 1-3 to add specific months and dates in the x-axis, shown below. However, the right y-axis should be PM mass concentration for both time series of $PM_{2.5}$ and PM_{10} concentration has been plotted.

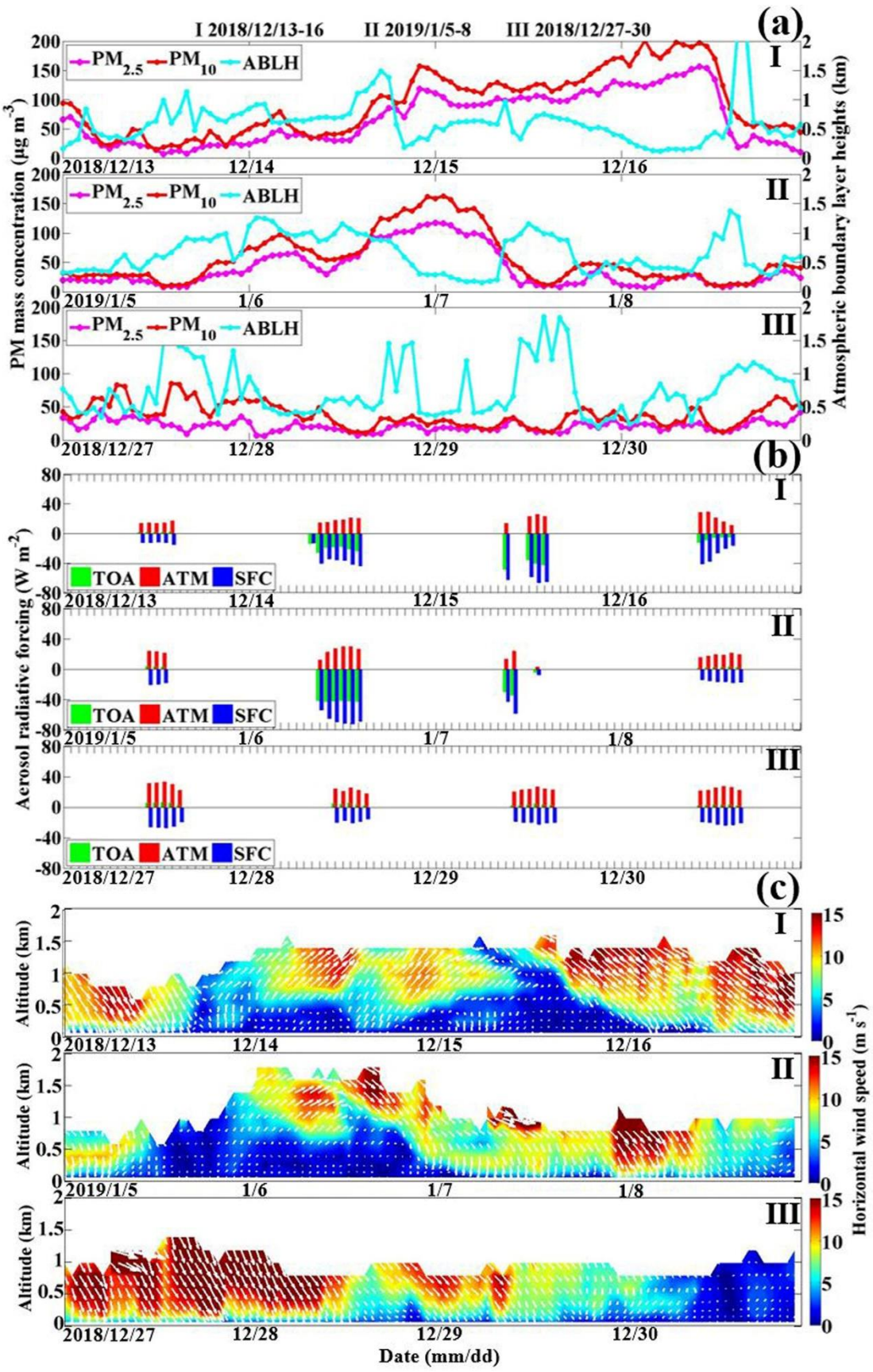

Figure 1. Temporal evolution of (a) the PM mass concentration and atmospheric boundary layer height ($PM_{2.5}$: solid pink lines; PM_{10}: solid red lines; ABLH: solid blue

lines), (b) aerosol radiative forcing at the top (TOA; green bars), surface (SFC; blue bars) and interior of the atmospheric column (ATM; red bars), and (c) horizontal wind vector profiles (shaded colors: wind speeds; white arrows: wind vectors) during the typical haze pollution episodes of I (2018/12/13-16) and II (2019/1/5-8) as well as the typical clean period of III (2018/12/27-30).

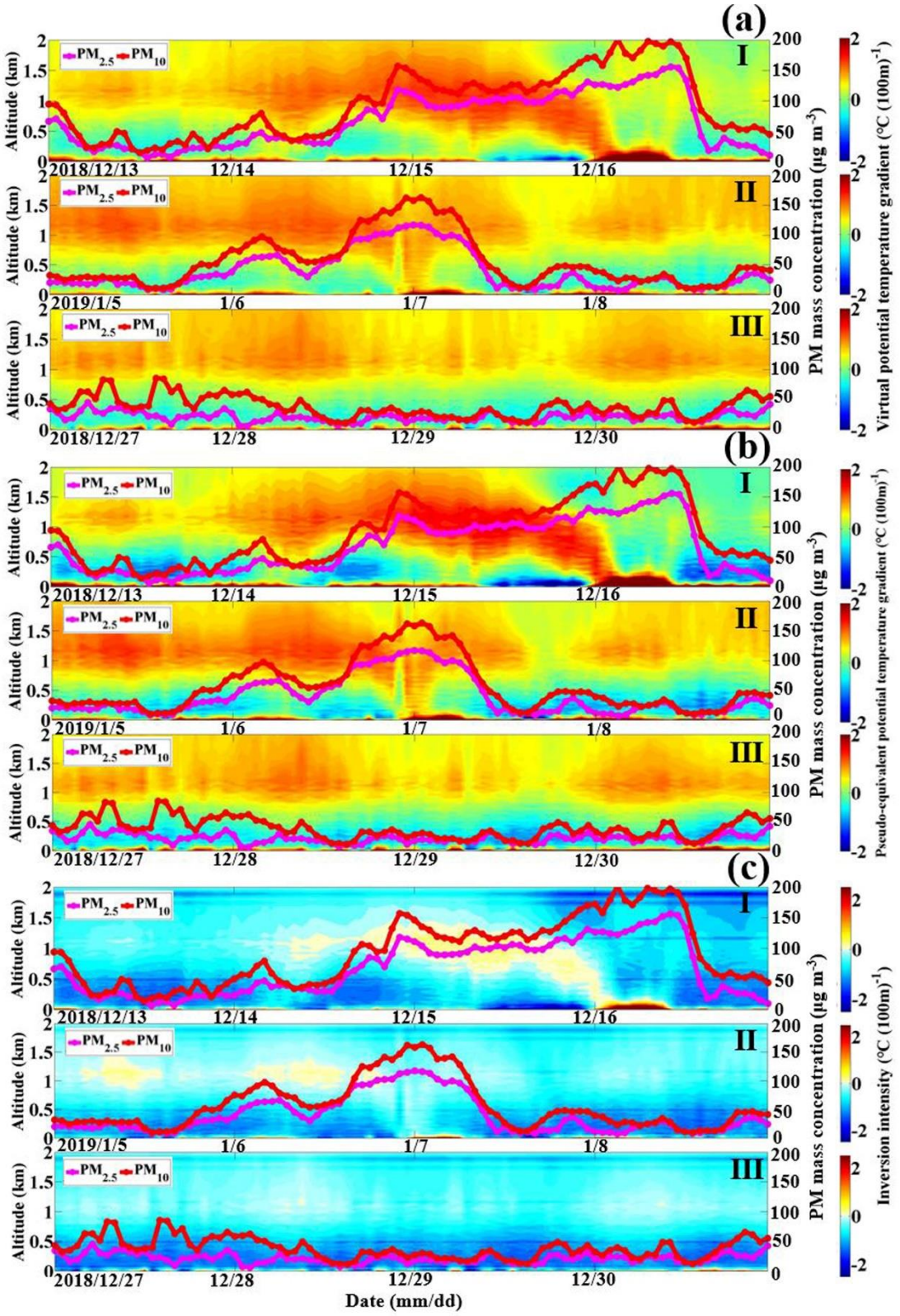

Figure 2. Temporal variation in the vertical profiles of (a) the virtual potential temperature gradient ($\partial\theta v/\partial z$), (b) pseudoequivalent potential temperature gradient ($\partial\theta se/\partial z$) and (c) temperature inversion phenomenon (shaded colors: inversion intensity) during the typical haze pollution episodes of I (2018/12/13-16) and II (2019/1/5-8) as well as the typical clean period of III (2018/12/27-30).

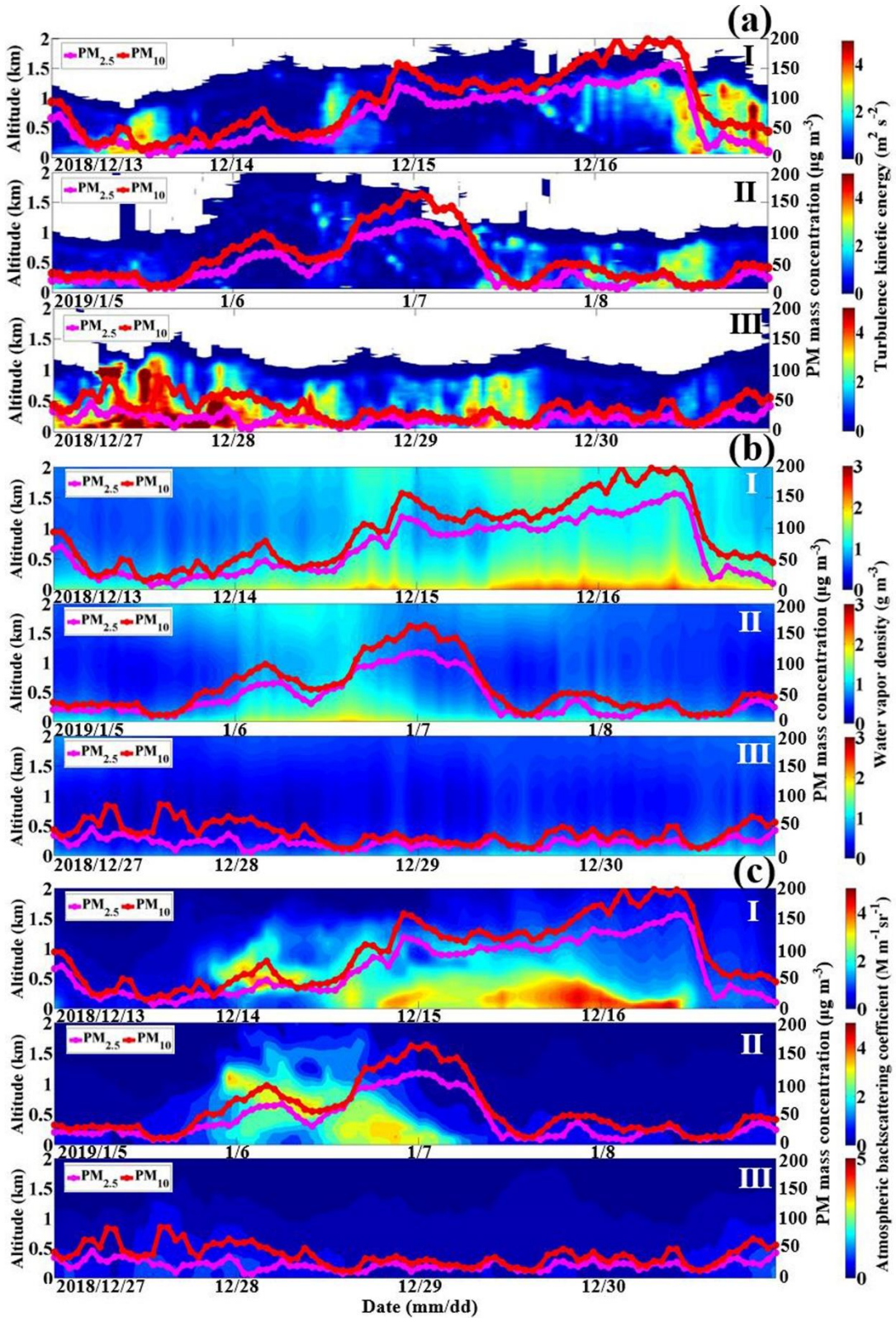

Figure 3. Temporal variation in the vertical profiles of (a) the turbulent activity (shaded colors: TKE), (b) atmospheric humidity (shaded colors: vapor density) and (c) vertical distribution of suspended particles (shaded colors: BSC) during the typical haze

pollution episodes of I (2018/12/13-16) and II (2019/1/5-8) as well as the typical clean period of III (2018/12/27-30).

5. Fig.3a: Usually, higher $PM_{2.5}$ concentrations, lower surface-reaching shortwave radiation, and weaker turbulent activity (i.e., lower TKE). However, such a relationship is not clear in the ABL on day 1 for Episode II and day 4 for Episode III.

Response: Thank the reviewer very much for this comment. Usually, in the daytime of the clean day, with the mixing layer developing the turbulent activity would be strong. In the ABL on day 1 for Episode II and day 4 for Episode III, the $PM_{2.5}$ concentrations were really low while the turbulent activity (i.e., lower TKE) was not too strong. Both mechanical and thermal actions determine turbulence activity. The wind fields during day 1 for Episode II and day 4 for Episode III were relatively weak, while the other clean periods were always corresponding to strong winds. With little mechanical action on turbulence generation, the TKE during these periods were not as strong as other clean periods.

6. L250-251, For the statement of "the atmospheric stratification during Episodes I and II was altered", please provide specific calculation to illustrate how the stratification was altered". Similar statements were also found in several places in the manuscript.

Response: Thank the reviewer very much for this comment. Regarding the statement "the atmospheric stratification during Episodes I and II was altered" in line 250-251 was concluded based on the previous analysis. The specific description is shown below:

"During the remainder of the 2nd day, the PM mass concentration continued to increase with south winds blowing and reached its highest level at midnight with a $PM_{2.5}/PM_{10}$ mass concentration of ~110/150 μg m^{-3} during both episodes I and II. The highest BSC values mainly occurred from the ground to a height of 1 km at this time, implying that a portion of the suspended particles was pushed down to the near-surface. *Noteworthily, regardless of the wind field, the atmospheric stratification states during this rising phase changed more notably. Before southerly wind transport occurred, the evolution of the stability indicator (∂θv/∂z; ∂θse/∂z) profiles during episodes I and II was analogous to that during episode III (Figs. 2(a)- (b)). The stratification states at the different heights (0-1 km) were either unstable or neutral, with negative or zero ∂θv/∂z values, respectively, whereby no clear nor strong temperature inversion phenomenon occurred in the lower atmosphere layer (Fig. 2(c)). The corresponding ABLHs were the same (Fig. 1(a)). However, the atmospheric stratification from ~0.5-1 km during the episode I and from 0-1 km during episode II became quite stable during the PM increase period, with positive values of ∂θse/∂z and almost no turbulent activity (TKE: ~0 m^2 s^{-2}) (Fig. 3(a)). In contrast to an increased ABLH during clean period III, the ABLHs during episodes I-II sharply decreased.* Considering that aerosol scattering and absorbing radiation could modify the temperature stratification (Li et al., 2010; Zhong et al., 2018), the aerosol radiation effect is too weak at a low PM level to change the latter, which defines the atmospheric stability. With the elevated PM level due to southerly transport, ARF also increased, with SFC (ATM) reaching ~-40 (~20) W m^{-2}

and ~-75 (~30) W m^{-2} during episodes I and II, respectively. Less radiation reaching the ground and more heating the atmosphere above the ground, and in comparison to clean episode III, the atmospheric stratification during episodes I and II was altered".

As described above, with the PM rising and the ARF increasing in episodes I and II, the corresponding atmospheric stratifications were altered compared to that in clean episode III and the previous no PM rising period.

7. Fig.4: It is difficult to understand that aerosol radiative forcing at top of the atmospheric column (TOA) has so close relationship with surface $PM_{2.5}$ concentrations. Please provide an explanation. Again, it is better to calculate the ARF for the integrated ABL rather than the interior of the atmospheric column.

Response: Thank the reviewer very much for this comment. As shown in Fig. 4(a), TOA forcing was proportional to the $PM_{2.5}$ concentration. With the increase in $PM_{2.5}$ concentration, elevated aerosol loading near the surface would scatter more solar radiation back into outer space and cause less solar radiation reaching the ground, corresponding to a cooling of the surface and making negative SFC. TOA means the aerosol radiative forcing at the top of the atmosphere column and is the sum of ATM and SFC. Considering that anthropogenic aerosols are mostly scattering aerosols, the SFC forcing is generally stronger than ATM, corresponding to a cooling of the earth-atmosphere system. The TOA forcing was thus usually negative and had a similar trend with SFC. The ARF calculation for the interior of the atmospheric column rather than the integrated ABL has been explained in Question 1.

8. Why did the authors use the absolute value of difference between SFC and ATM? Why not use ATM–SFC since ATM is positive and SFC is negative? In fact, the ATM-SFC represent a combined impact of aerosol radiative effect on surface-reaching shortwave radiation and the atmospheric layer. It is not surprised to see ATM-SFC increases with increasing $PM_{2.5}$ concentrations (see Fig. 4d). Here the authors still use scatter plots to quantify the relationship between aerosol radiative effect and surface $PM_{2.5}$ in terms of model results. Are there any observational data available to verify the results?

Response: Thank the reviewer very much for this comment. First of all, we all know that the difference between SFC and ATM means a combined impact of the aerosol radiative effect on surface-reaching shortwave radiation and the atmospheric layer. The reason we use the absolute value of SFC-ATM is that ATM is positive and SFC is negative; thus the SFC- ATM is always negative. The absolute value of SFC-ATM represents the same meaning as ATM-SFC. Secondly, we plotted this scatter plot (Fig. 4d) to show the relationship between the combined impact of the aerosol radiative effect on surface-reaching shortwave radiation and the atmospheric layer and $PM_{2.5}$ concentrations. It shows |SFC-ATM| increases with increasing $PM_{2.5}$ concentrations. We need to explain that the aerosol radiative forcing (ie., SFC and ATM) can be obtained only by models. Regarding the observational data verify, Zhong et al. (2018) once verified the relationship between the global radiant exposure measured at the

surface and $PM_{2.5}$ concentrations, shown as below. To further investigate the impact of elevated $PM_{2.5}$ on the loss in surface solar radiation, they calculated daytime mean $PM_{2.5}$ mass concentration, direct, diffuse, and global radiant exposure in December 2016 to 10th January 2017 in Beijing. We can see that the radiation reaching the ground decreased with the $PM_{2.5}$ concentration increasing, consistent with the relationship between SFC and $PM_{2.5}$ concentration in Fig. 4(c). However, the radiation in the atmosphere is hard to be measured yet. Thus, the aerosol radiative effect on the earth-atmosphere system is mainly based on the aerosol radiative forcing calculated by models.

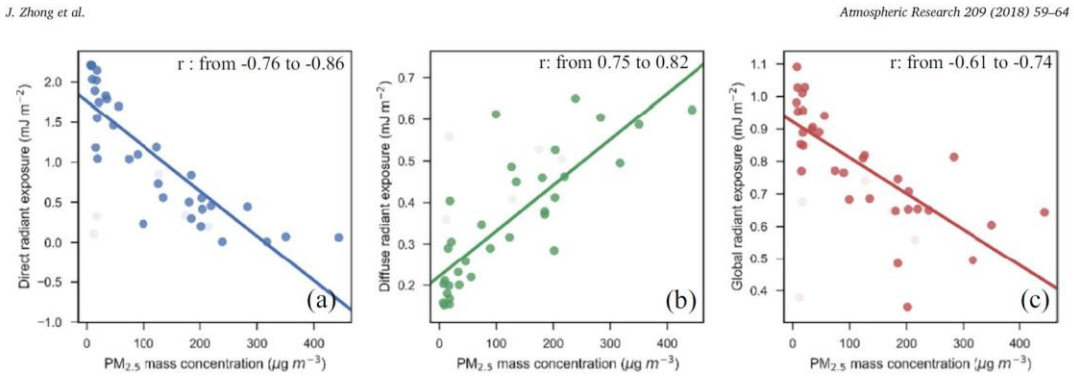

Fig. 2. The correlation of daytime mean $PM_{2.5}$ mass concentration and daytime mean radiant exposure from 1st December 2016 to 10th January 2017. (a) $PM_{2.5}$ and direct radiant exposure; (b) $PM_{2.5}$ and diffuse radiant exposure; (c) $PM_{2.5}$ and global radiant exposure; (semitransparent points represents the days with high-layer moisture, and r shows the variations without semitransparent points).

Zhong J., Zhang X., Wang Y., Liu C., and Dong Y.: Heavy aerosol pollution episodes in winter Beijing enhanced by radiative cooling effects of aerosols, Atmos. Res., 59-64, 10.1016/j.atmosres.2018.03.011, 2018.

9. Fig.6: Please add a), b), c), and d) each panel, respectively, and specify clearly in the figure caption.

Response: Thank the reviewer very much for this suggestion. We have added a), b), c), and d) each panel, respectively, and specify clearly in the figure caption, shown below.

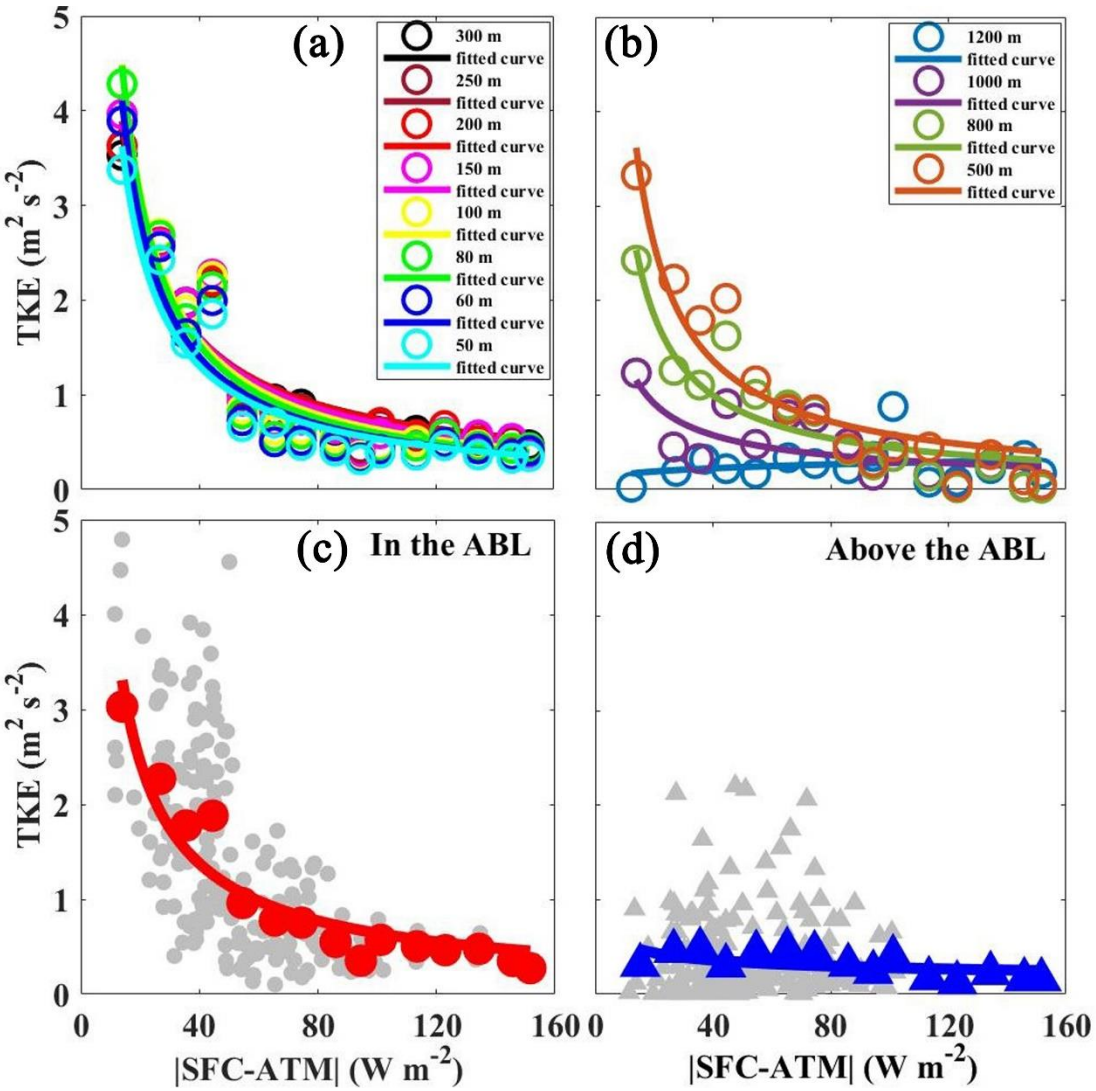

Figure 6. Scatter plots of the mean absolute difference of the aerosol radiative forcing at the surface and interior of the atmospheric column (|SFC-ATM|; x) versus the mean turbulence kinetic energy (TKE; y) at the different altitudes (a; b). Scatter plots of |SFC-ATM| (x) versus TKE (y) in the ABL (c) and above the ABL (d) (gray dots: hourly data; other dots: mean data). The hourly data were collected over a two-month period in Beijing from 27 November 2018 to 25 January 2019. (The hourly data means hourly mean values of |SFC-ATM| and corresponding hourly TKE. The mean |SFC-ATM| was obtained by averaging hourly |SFC-ATM| at intervals of 10 W m^{-2}, then the mean TKE was obtained after the average of the corresponding hourly TKE.).

10. L87-91: This is definitely not true if the authors claimed that "this paper is the first time to analyze the interaction between ….". Many studies have devoted to understanding and quantifying the interactions between aerosol radiative effect and the atmospheric boundary layer thermodynamic and dynamic structures up to now. Some examples include Zhao et al., 2019, Zhang et al., 2020, Miao et al., 2020, Liu et al. 2020, etc.

Response: Thank the reviewer very much for this suggestion. This kind of mistake has

been pointed out, and we have corrected it in the first referee round. We thank the reviewer again for pointing out this problem and have modified it.

11. Line 510: Again, this study is definitely not the first one. Please delete any statement like this.

Response: We thank the reviewer again for pointing out this problem, and we have modified it.

12. L15: I am very concerned with the statement with "…because most studies have been superficial". Please delete or modify it.

Response: Thank the reviewer very much for this suggestion. This kind of mistake has been pointed out, and we have corrected it in the first referee round. We thank the reviewer again for pointing out this problem and have modified it.

Marked-up manuscript:

The impact threshold of the aerosol radiation forcing on the boundary layer structure in the pollution region

Dandan Zhao[†1,2], Jinyuan Xin[*†1,2], Chongshui Gong[3], Jiannong Quan[4], Yuesi Wang[1,2], Guiqian Tang[1], Yongxiang Ma[1], Lindong Dai[1], Xiaoyan Wu[1], Guangjing Liu[1], Yongjing Ma[1]

1 State Key Laboratory of Atmospheric Boundary Layer Physics and Atmospheric Chemistry (LAPC), Institute of Atmospheric Physics, Chinese Academy of Sciences, Beijing 100029, China

2 University of Chinese Academy of Sciences, Beijing 100049, China

3 Institute of Arid Meteorology, China Meteorological Administration, Lanzhou 730020, China

4 Institute of Urban Meteorology, Chinese Meteorological Administration, Beijing, China

(†) These authors contributed equally to this study.

(*) Correspondence: Jinyuan Xin; email: xjy@mail.iap.ac.cn; phone: (+86)15810006545; address: #40 Huayanli, Chaoyang District, Beijing 100029, China

Abstract: Recently, there has been increasing interest in the relation between particulate matter (PM) pollution and atmospheric boundary layer (ABL) structure. However, this topic has yet to be fully understood. This study aimed to qualitatively assess the interaction between PM and ABL structure in essence and further quantitatively estimate aerosol radiative forcing (ARF) effects on the ABL structure. Multi-period comparative analysis indicated that the key to determining whether the haze outbreak or dissipation occurs is whether the ABL structure (i.e., stability and turbulent

kinetic energy (TKE)) satisfies the relevant conditions. However, the ABL structure change was in turn highly related to the PM level and ARF. |SFC-ATM| (SFC and ATM are the ARFs at the surface and interior of the atmospheric column, respectively) is the absolute difference between ground and atmosphere layer ARFs, and the |SFC-ATM| change is linearly related to the PM concentrations. However, the influence of ARF on the boundary layer structure is nonlinear. With increasing |SFC-ATM|, the TKE level exponentially decreased, which was notable in the lower layers/ABL but disappeared at high altitudes/above the ABL. Moreover, the ARF effects threshold on the ABL structure was determined for the first time, namely, once |SFC-ATM| exceeded ~ 55 W m^{-2}, the ABL structure would quickly stabilize and would thereafter change little with increasing ARF. The threshold of the ARF effects on the boundary layer structure could provide useful information for relevant atmospheric environment improvement measures and policies, such as formulating phased air pollution control objectives.

Keywords: boundary layer structure; aerosol radiative forcing; threshold; haze pollution

1 Introduction

Most areas in China, such as the North China Plain, have suffered from poor air quality due to rapid economic growth. Beijing, as the Chinese capital and principal city in the North China Plain, has frequently experienced severe and persistent haze events, characterized by an exceedingly high particulate matter (PM) mass loading suspended in near-surface air (Li et al., 2020; Wang et al., 2018; Xu et al., 2019; Zhong et al., 2018). As previous studies have found, air pollution episodes are the result of secondary aerosol formation and adverse meteorological conditions (An et al., 2019; Guo et al., 2014; Li et al., 2017; Wang et al., 2014; Zheng et al., 2015; Wang et al., 2012). PM is concentrated in the atmospheric boundary layer (ABL) (Petaja et al., 2016; Tie et al., 2017), which is the lower part of the troposphere and is directly affected by the surface (Quan et al., 2013). The diffusion, transmission, and accumulation of pollutants are closely linked to ABL structure (meteorological conditions) variation (Han et al., 2009; Kotthaus and Grimmond, 2018; Zheng et al., 2017). Numerous studies have revealed that the meteorological factors in the boundary layer influence the formation of air

pollution periods (Hua et al., 2016; Liu et al., 2016; Miao et al., 2018; Wang et al., 2012; Wang et al., 2014; Zhang et al., 2018). For instance, the aerosols concentrated in the ABL exhibit a strong negative relationship with the ABL height (ABLH) that determines the volume available for pollutant dispersion (Haman et al., 2014; Schaefer et al., 2009; Su et al., 2018; Tang et al., 2016). Heavy air pollution episodes have always occurred with persistent temperature inversions (Xu et al., 2019; Zhong et al., 2017). Weak/calm winds are essential in the long-term increase in air pollutants (Niu et al., 2010; Yang et al., 2016). Additionally, previous studies have reported that severe air pollution is always positively related to high atmospheric humidity, one of the manifestations of stagnant ABL conditions (Tie et al., 2017; Petaja et al., 2016). Moreover, the feedback/interaction mechanism between the boundary layer structure and aerosol loading during severe pollution events has been analyzed in previous studies (Huang et al., 2018; Liu et al., 2018; Zhong et al., 2018b; Zhong et al., 2019; Zhao et al., 2019).

However, most of the work was performed through a relationship analysis of the PM concentration and meteorological factors and mainly considered specific pollution processes. Few attempts have been made to examine the interaction between the ABL and air pollution in essential aspects. Since the surface directly influences the ABL, it is the only atmosphere layer characterized by turbulent activities, while higher atmosphere layers are weakly turbulent because of the strongly stable stratification (Munro, 2005). Thus, the ABL acts as a notable turbulence buffer coupling the surface with the free atmosphere, and PM and gas pollutants are only suspended in the ABL and are convectively spread throughout it. The evolution of the ABL structure, which plays a key role in pollutant accumulation/diffusion, is substantially the change in turbulent kinetic energy (TKE) in the ABL (Garratt et al., 1992). Therefore, we systematically analyzed the way the ABL interacts with pollutants via contrastive analysis of multiple haze episodes based on not only specific meteorological factors but also turbulent activity profiles and atmospheric stability indicators. Moreover, the change in solar radiation reaching the ground drives the diurnal ABL evolution considering atmospheric stability variation (Andrews, 2000). The diurnal evolution of

the atmospheric thermodynamic status is greatly affected considering a strong aerosol radiative effect, namely strongly scattering radiation and/or absorbing radiation, occurs on severe air pollution (Dickerson et al., 1997; Liu et al., 2018; Huang et al., 2018; Stone et al., 2008; Zhong et al., 2018a). As previous studies have reported, the aerosol radiative forcing (ARF), used to quantify the aerosol radiation effects, is a critical parameter that can further modify the boundary layer structure during haze episodes (Gong et al., 2014). Ding et al. (2016) and Wilcox et al. (2016) demonstrated that the highly absorptive black carbon aerosol with strong absorption ability could notably enhance atmospheric stability and suppress boundary layer development. While an increase of aerosol scattering effect also led to a decrease of ABL height (ABLH) (Barbaro et al., 2014; Yu et al., 2002). Petäjä et al. (2016) also suggested that the synergistic scattering (surface cooling) and absorption (atmospheric heating) effects modify the vertical temperature stratification. However, the influence degree of the aerosol radiative effect on the boundary layer structure remains unclear. Quantitatively determining the effects of ARF on the ABL structure is urgently needed. Furthermore, this paper would analyze the interaction between the ABL structure and air pollution using high-resolution and real-observation datasets, such as temperature and humidity profiles of microwave radiometers, horizontal and vertical wind vector profiles of Doppler wind lidar, ABLH, and aerosol backscattering coefficient profiles of ceilometers. Wind profile lidar and microwave radiometers have the advantage of providing direct and continuous observations of the boundary layer over long periods and can characterize the ABL structure up to 2-3 km (Pichugina et al., 2019; Zhao et al., 2019), compensating for the deficiencies of previous research.

2 Data and methods

We conducted a two-month measurement campaign of the PM concentration and aerosol optical depth (AOD) and obtained vertical profiles of atmospheric parameters such as temperature, humidity, wind vectors, atmospheric stability, and TKE to better understand how the boundary layer structure responds to aerosol radiative effects. Figure S1 shows the observation site of the Tower Branch of the Institute of

Atmospheric Physics (IAP), Chinese Academy of Sciences (39° 58′ N, 116° 22′ E; altitude: 58 m) and the sampling instruments in this study. The IAP site represents a typical urban Beijing site, and all the sampling instruments are placed at the same location, and simultaneous monitoring is conducted. The algorithm of SBDART (Santa Barbara DISORT Atmospheric Radiative Transfer) (Levy et al., 2007) is the core model to calculate the radiative forcing parameters. A standard mid-latitude atmosphere is used in SBDART in Beijing. AOD and Angstrom Exponent (AE) at 550 nm were obtained from a sun-photometer. Multiple sets of Single Scattering Albedo (SSA) and backscattering coefficient were calculated based on MIE theory, and surface albedo & path radiation were read from MODIS (MOD04), which is used to calculate radiative forcing at the top of atmosphere (TOA). The TOA results were combined with MODIS observations, the result which has the lowest deviation are defined as the actual parameters of aerosols, and this set of parameters would be used to calculate the radiative forcing at the surface, top, and interior of the atmospheric column (Gong et al., 2014; Lee et al, 2018; Xin et al., 2016). Hourly radiative forcing parameters, including the ARF at the top (TOA), surface (SFC), and interior of the atmospheric column (ATM) at an observation site in Beijing can be calculated based on this algorithm. More detailed descriptions are provided in our previous work (Gong et al., 2014; Lee et al, 2018; Xin et al., 2016).

Air temperature and relative and absolute humidity profiles were retrieved with a microwave radiometer (after this referred to as MWR) (RPG-HATPRO-G5 0030109, Germany). The MWR produces profiles with a resolution ranging from 10-30 m up to 0.5 km, profiles with a resolution ranging from 40-70 m between 0.5 and 2.5 km, and profiles with a resolution ranging from 100-200 m from 2 to 10 km at a temporal resolution of 1 s. More detailed information on the RPG-HATPRO-type instrument can be found at http://www.radiometer-physics.de (last access: 4 June 2020). Vertical wind speed and horizontal wind vector profiles were obtained by a 3D Doppler wind lidar (Windcube 100s, Leosphere, France). The wind measurement results have a spatial resolution ranging from 1-20 m up to 0.3 km and a spatial resolution of 25 m from 0.3 to 3 km, at a temporal resolution of 5 s. More instrument details can be found at

www.leosphere.com (last access: 4 June 2020). A ceilometer (CL51, Vaisala, Finland) was adopted to acquire atmospheric backscattering coefficient (BSC) profiles. The CL51 ceilometer digitally receives the return backscattering signal from 0 to 100 μs and provides BSC profiles with a spatial resolution of 10 m from the ground to a height of 15 km. The ABLH was further identified by the sharp change in the BSC profile's negative gradient (Münkel et al., 2007), and detailed information is reported in previous studies (Tang et al., 2015, 2016; Zhu et al., 2018). A CIMEL sun-photometer (CE318, France), a multichannel, automatic sun-and-sky scanning radiometer (Gregory 2011), was used to observe the AOD, and the AOD at 500 nm is adopted in this paper. The real-time hourly mean ground levels of $PM_{2.5}$ (particulate matter with aerodynamic diameter less than or equal to 2.5 μm) and PM_{10} (particulate matter with aerodynamic diameter less than or equal to 10 μm) were downloaded from the China National Environmental Monitoring Center (CNEMC) (available at http://106.37.208.233:20035/, last access: 4 June 2020).

The virtual potential temperature (θ_V) and pseudoequivalent potential temperature (θ_{se}) are calculated with Eqs. (1) and (2), respectively:

$$\theta_{\mathrm{v}} = T(1 + 0.608q)\left(\frac{1000}{P}\right)^{0.286} \quad (1)$$

$$\theta_{se} = T\left(\frac{1000}{P}\right)^{0.286} exp\left(\frac{r_s L_v}{C_{pd} T}\right) \quad (2)$$

where T is the air temperature, q is the specific humidity, p is the air pressure, r_s is the saturation mixing ratio, Lv is the latent heat of vaporization at 2.5×10^6 J kg^{-1}, and C_{pd} is the specific heat of air at 1005 J kg^{-1} K^{-1}. All the relevant parameters can be calculated from the temperature and humidity profile data obtained with the MWR, and the values of θ_v and θ_{se} at different altitudes can be then further obtained. The hourly TKE is calculated by instantaneous three wind components sampled by Doppler wind lidar every five seconds (shown as Equation (3)-(6)). The calculated TKE profile has a spatial resolution ranging from 1-20 m up to 0.3 km and a spatial resolution of 25 m from 0.3 to 3 km, at a temporal resolution of one hour.

$$\mathrm{TKE} = 0.5 \times (\delta_u^2 + \delta_v^2 + \delta_w^2). \quad (3)$$

The one-hour vertical velocity standard deviation (δ_w^2) and one-hour horizontal wind

standard deviation (δ_u^2; δ_v^2) are calculated with Eqs. (4), (5) and (6), respectively:

$$\delta_w^2 = \frac{1}{N-1}\sum_{i=1}^{N}(w_i - \bar{w})^2 \quad (4)$$

$$\delta_u^2 = \frac{1}{N-1}\sum_{i=1}^{N}(u_i - \bar{u})^2 \quad (5)$$

$$\delta_v^2 = \frac{1}{N-1}\sum_{i=1}^{N}(v_i - \bar{v})^2 \quad (6)$$

where N is the number of records per hour, w_i is the i_{th} vertical wind velocity (m s^{-1}), $u_i(v_i)$ is the i_{th} horizontal wind speed (m s^{-1}), $\bar{w}$ is the mean vertical wind speed (m s^{-1}), and $\bar{u}$ ($\bar{v}$) is the mean horizontal wind speed (m s^{-1}) (Banta et al., 2006; Wang et al., 2019).

3 Results and discussion

3.1 General haze episodes over Beijing in winter

It is well known that severe air pollution episodes frequently occur in Beijing during autumn and winter (Jin-Xiang, 2007; Zhang et al., 2017). Two-month PM concentration data from Beijing in the winter of 2018 were collected. As expected, during this time, Beijing experienced severe and frequent haze pollution episodes with two heavy episodes in which the maximum hourly $PM_{2.5}$ concentration reached ~200 μg m^{-3} and six available episodes in which the $PM_{2.5}$ mass concentration ranged from ~100-150 μg m^{-3} (Fig. S2(a)). Although the air pollution process is variable and complicated, it is worth stating that Beijing's haze pollution in winter can be generally classified as two kinds of patterns, as shown in Fig. S2(b). For all haze episodes ①-⑦, the $PM_{2.5}$ mass concentration slowly increased in the afternoon of the first day, followed by a secondary maximum in the early morning and a maximum at midnight of the second day. In comparison to the processes of ④-⑦, where the $PM_{2.5}$ mass concentration sharply decreased to <25 μg m^{-3} in the early morning of the third day, during periods ①-③, however, the highest $PM_{2.5}$ mass concentration (~100-200 μg m^{-3}) was observed on the third day, which disappeared on the fourth day. As previously reported, transport, physical and chemical transformation and boundary layer structure (local meteorological conditions) are central to determining the amount and type of pollutant loading. The suspended particles in ④-⑦ were subjected to dispersal, controlled by the atmospheric motion (wind and turbulence) on the third day. The particles during

periods ①-③ continued to accumulate and were therefore highly related to the specific ABL status. To investigate the possible reasons for the different variation trends of haze episodes ①-③ and ④-⑦, in the next section, we will mainly focus on the ABL structure (local meteorological conditions) considering transport and physical and chemical transformation.

3.2 Qualitative analysis of the interaction between particulate matter and boundary layer structure

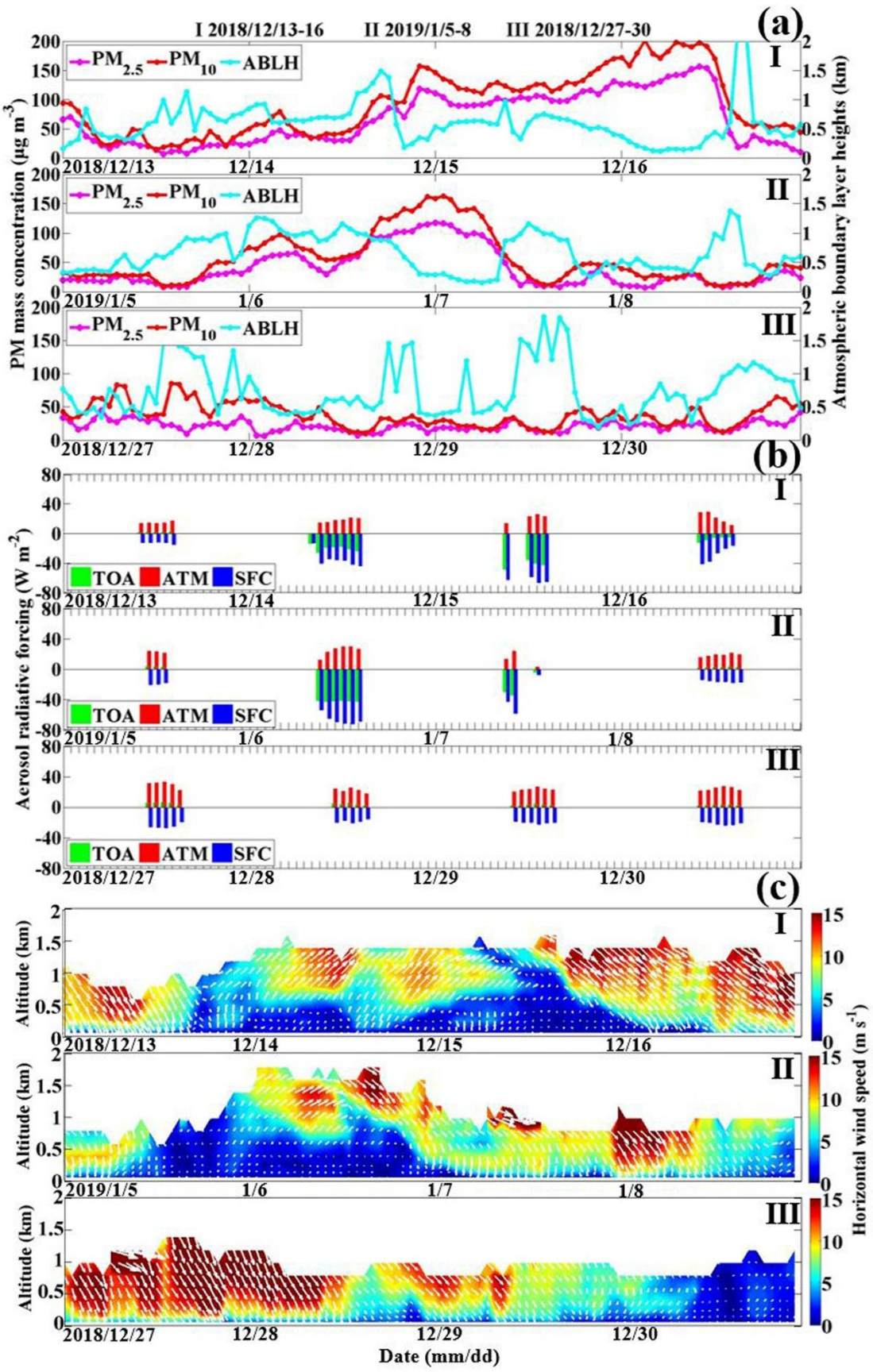

Figure 1. Temporal evolution of (a) the PM mass concentration and atmospheric boundary layer height ($PM_{2.5}$: solid pink lines; PM_{10}: solid red lines; ABLH: solid blue

lines), (b) aerosol radiative forcing at the top (TOA; green bars), surface (SFC; blue bars) and interior of the atmospheric column (ATM; red bars), and (c) horizontal wind vector profiles (shaded colors: wind speeds; white arrows: wind vectors) during the typical haze pollution episodes of I (2018/12/13-16) and II (2019/1/5-8) as well as the typical clean period of III (2018/12/27-30).

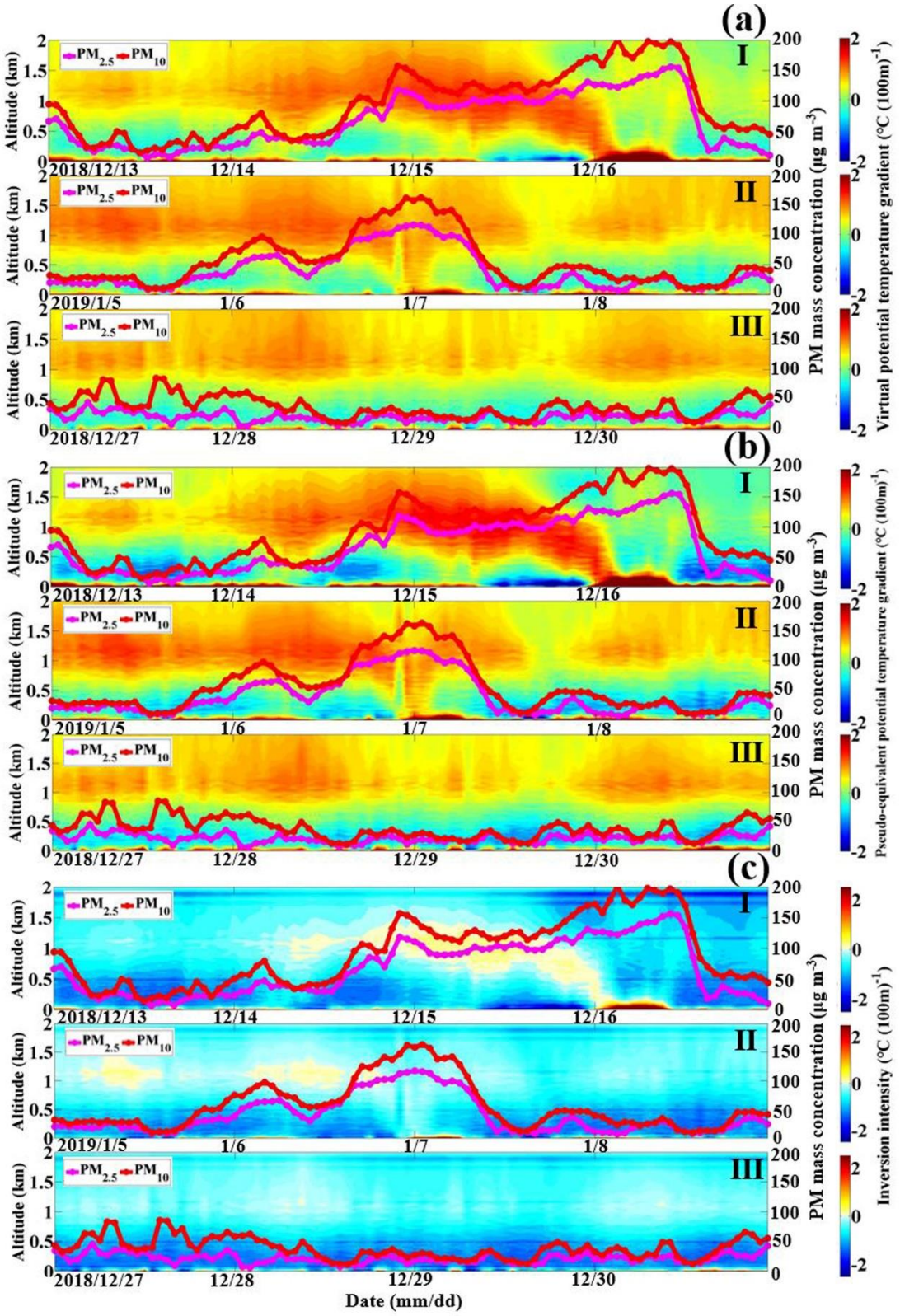

Figure 2. Temporal variation in the vertical profiles of (a) the virtual potential temperature gradient ($\partial\theta v/\partial z$), (b) pseudoequivalent potential temperature gradient ($\partial\theta se/\partial z$) and (c) temperature inversion phenomenon (shaded colors: inversion intensity) during the typical haze pollution episodes of I (2018/12/13-16) and II (2019/1/5-8) as

well as the typical clean period of III (2018/12/27-30).

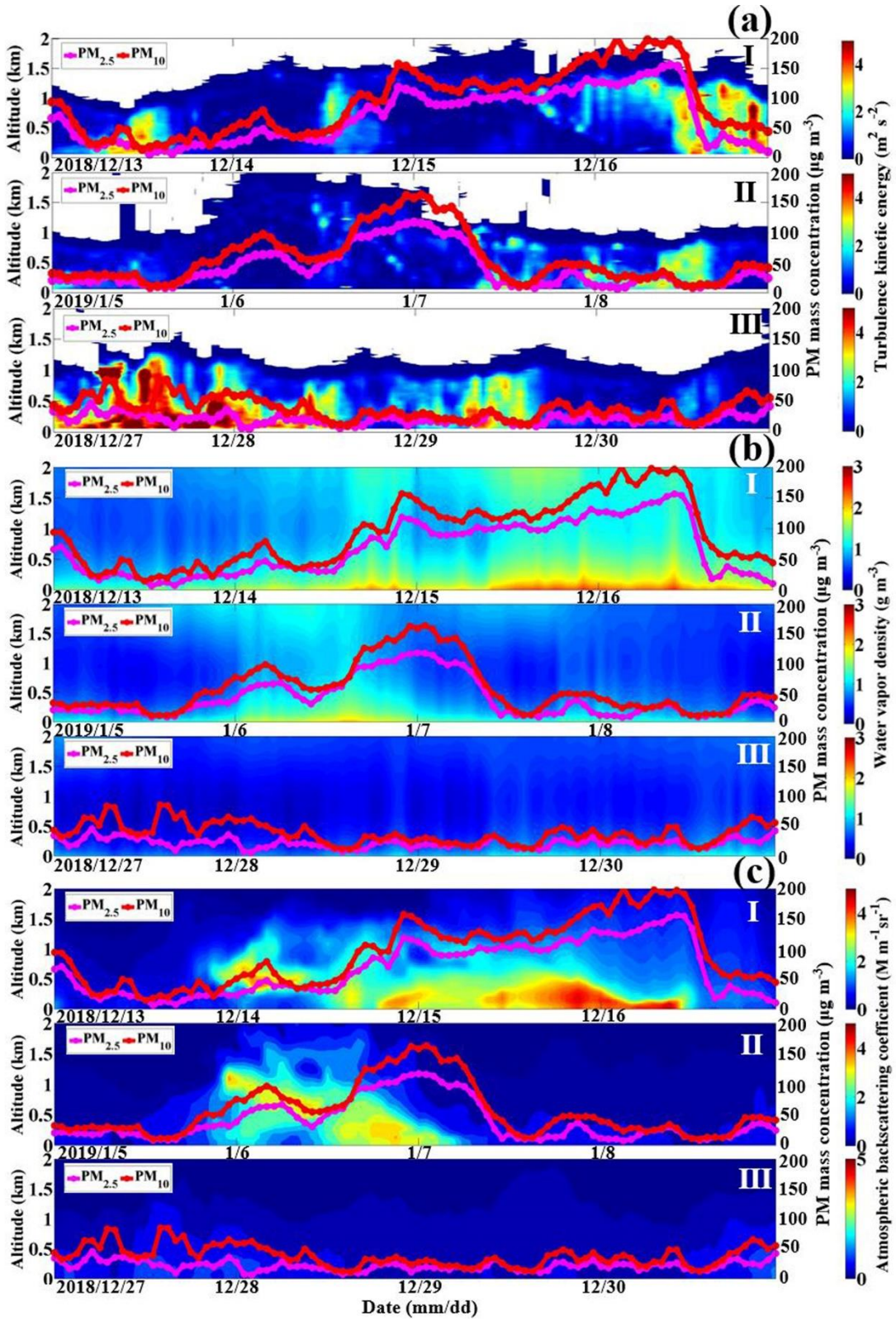

Figure 3. Temporal variation in the vertical profiles of (a) the turbulent activity (shaded colors: TKE), (b) atmospheric humidity (shaded colors: vapor density), and (c) vertical distribution of suspended particles (shaded colors: BSC) during the typical haze

pollution episodes of I (2018/12/13-16) and II (2019/1/5-8) as well as the typical clean period of III (2018/12/27-30).

Although not exactly the same, the haze episodes followed two different kinds of variation trends as described in the previous section. The specific reason for this finding will be systematically analyzed in this section. To better illustrate the two different haze pollution patterns, a typical clean period will be considered a control. The typical air pollution episodes of I (2018/12/13-16) and II (2019/1/5-8), as well as the typical clean period of III (2018/12/27-30), are chosen as examples for analysis. Numerous studies have reported that PM's original explosive growth is caused by pollution transport under southerly winds (Ma et al., 2017; Zhao et al., 2019; Zhong et al., 2018). In this study, the action of southerly winds on the air pollution in Beijing was presented more clearly as the Windcube 100s lidar obtained the distribution of the horizontal wind vectors extending to heights of 1-1.5 km (equivalent to the entire ABL) (Fig. 1(c)). On the 1st day of episodes I and II, the atmosphere layer up to ~1 km in height was controlled by strong and clean north winds, exactly like clean period III. No pollution transport occurred, and the PM and ARF levels were equivalent to those on a clean day (Figs. 1(a)-(b)). The atmospheric backscattering coefficients throughout the ABL during the three episodes only ranged from ~0-1.5 M $m^{-1}sr^{-1}$ (Fig. 3(c)). From the evening of the 1st day to the forenoon of the 2nd day, strong southerly winds blew across Beijing during both episodes I and II, with the wind speed increasing with the height, reaching ~5-15 m s^{-1} at an atmosphere of about 0.5-1.5 km. North winds still dominated the ABL during clean episode III. Sensitive to the change in wind direction from north to south, the PM mass concentration progressively increased from a fairly low level to ~50 μg m^{-3}. Moreover, the BSCs sharply increased to ~3 Mm^{-1} rd^{-1} and were concentrated at altitudes from ~0.5-1 km, which further stressed the effects of southerly transport on the PM mass concentration's original growth over Beijing. With winds originating from the wetter south, compared to the low humidity during clean episode III, the air humidity in Beijing during this time notably increased with the vapor density ranging from ~1.5-2 g m^{-3} during both episodes I and II (Fig. 3(b)). During the remainder of the 2nd day, the PM mass concentration increased with south winds blowing and reached

its highest level at midnight with a $PM_{2.5}/PM_{10}$ mass concentration of ~110/150 μg m^{-3} during both episodes I and II. The highest BSC values mainly occurred from the ground to a height of 1 km at this time, implying that a portion of the suspended particles was pushed down to the near-surface. Noteworthily, regardless of the wind field, the atmospheric stratification states during this rising phase changed more notably. Before southerly wind transport occurred, the evolution of the stability indicator ($\partial\theta_v/\partial z$; $\partial\theta_{se}/\partial z$) profiles during episodes I and II was analogous to that during episode III (Figs. 2(a)-(b)). The stratification states at the different heights (0-1 km) were either unstable or neutral, with negative or zero $\partial\theta_v/\partial z$ values, respectively, whereby no clear nor strong temperature inversion phenomenon occurred in the lower atmosphere layer (Fig. 2(c)). The corresponding ABLHs were the same (Fig. 1(a)). However, the atmospheric stratification from ~0.5-1 km during the episode I and from 0-1 km during episode II became quite stable during the PM increase period, with positive values of $\partial\theta_{se}/\partial z$ and almost no turbulent activity (TKE: ~0 m^2 s^{-2}) (Fig. 3(a)). In contrast to an increased ABLH during clean period III, the ABLHs during episodes I-II sharply decreased. Considering that aerosol scattering and absorbing radiation could modify the temperature stratification (Li et al., 2010; Zhong et al., 2018a), the aerosol radiation effect is too weak at a low PM level to change the latter, which defines the atmospheric stability. With the elevated PM level due to southerly transport, ARF also increased, with SFC (ATM) reaching ~-40 (~20) W m^{-2} and ~-75 (~30) W m^{-2} during episodes I and II, respectively. Less radiation reaching the ground and more heating the atmosphere above the ground, and in comparison to clean episode III, the atmospheric stratification during episodes I and II was altered. Besides, TOA has an analogous variation trend with SFC, increasing from relatively low values to ~-20 W m^{-2} and ~-45 W m^{-2} during episodes I and II, respectively. It further clarified the high scattering effect of aerosols with the elevated PM level. The suspended particles carried by southerly transport originally occurring at high altitudes were restrained from vertically spreading and gradually sank due to gravity and accumulated near the surface. This stable stratification has a certain impact on aggravating haze pollution.

It is salient to note that the haze evolution trends during episodes I and II were

consistent so far, corresponding to a similar ABL structure. Nevertheless, the north winds (~10-15 m s^{-1}) during episode II, which only blew above the ABL (>1 km) at midnight of the 2nd day, gradually spread downward and controlled the whole boundary layer on the 3rd day. Moreover, the south wind, which once was strong and filled the boundary layer on the 2nd day during the episode I, gradually decelerated over time from the ground to high altitudes on the 3rd day. The wind field is critical concerning horizontal dispersion in the boundary layer; thus, the strong, clean and dry north winds during episode II greatly diffused the already accumulated particles first, where the $PM_{2.5}$ mass concentration decreased from ~100 to ~50 μg m^{-3}. The ARF obtained at this time (at 9:00) also decreased compared to yesterday, and with solar radiation heating the ground in the morning on the 3rd day, the positive sensible heat flux (upward heat transfer) eliminated the previous night's temperature structure. The temperature stratification became similar to that on clean day III with a similar increase in ABLH. Thus, an unstable/neutral atmospheric state with a TKE of ~2 m^2 s^{-2} was also conducive to the vertical spread of materials replaced with cleaner air from above. In response, the PM mass concentration (BSC) and air humidity during episode II gradually decreased with the convective boundary layer development and reached the same level as those during episode III. During the time (from 9:00 to 13:00) when the ARFs can be obtained, the ARFs showed a consistent change with PM, gradually decreased to quite low levels. Conversely, the whole ABL (0-1 km) was controlled by calm/light winds during the episode I on the 3rd day. On account of the calm/light winds, the horizontal wind shear sharply decreased, resulting in a decline in mechanical turbulence intensity. In the absence of an existing high PM mass concentration, strong ARF would continue to cool the ground notably and heat the aerosol layer, keeping the atmospheric stratification stable and decreasing thermal turbulence intensity. As can be seen in Fig. 1(b), SFC and TOA further increased compared to yesterday, up to ~-40 W m^{-2} and ~-75 W m^{-2}, respectively, with ATM remaining higher (~25 W m^{-2}). And since the high PM concentration was relatively stable from 8:00 to 14:00 when the ARFs were obtained, the elevated ARFs also kept relatively fixed values during this time. This was different from that in case II and further indicated the sensitivity between PM concentrations and

ARFs. The ABLH barely changed on the 3rd day and maintained a lower altitude in the forenoon of the 4th day. Therefore, a rather stable atmosphere extended from ~0.3-0.5 km to ~1.5 km on the 3rd day and from the ground to heights of ~0.3 km in the forenoon of the 4th day (Figs. 2(a)-(c)). The quite low TKE was highly consistent with the atmospheric stability stratification. Since the stable stratification acted as a lid at altitudes from 0.5-1.5 km, downward momentum transport would be blocked, further explaining the lower atmosphere layer's calm/light winds. In the forenoon of the 4th day, it is worth noting that above the stable atmospheric stratification (0-0.3 km altitude), a relatively strong horizontal wind shear occurred corresponding to a TKE of ~1-2 $m^2 s^{-2}$. The accumulated particles near the surface were further inhibited right below the stable atmosphere layer, as reflected by the BSC distribution. This highlights that a stable atmosphere with a weak turbulent activity was central to pushing down the pollutant layer. The same work was exerted on the water vapor as the air humidity at this time reached ~3 g m^{-3} below an altitude of ~0.3 km, accompanied by intense heterogeneous hydrolysis reactions at the moist particle surface (Zhang et al., 2008), which further increased the PM mass concentration. At noon of the 4th day, north winds spread down to the whole ABL, which promoted the horizontal and convective dispersion of pollutants and water vapor, and the PM mass concentration, therefore, dropped to the same level as that on clean day III. With $PM_{2.5}$ sharply dropped from ~150 μg m^{-3} to ~20 μg m^{-3} in four hours, the aerosol radiative effect was sensitive to PM changes and gradually decreased from 10:00 to 14:00, reaching the same level as those on clean day III finally. For case II and III, the PM concentrations barely changed during the moment (from 10:00 to 14:00), the corresponding ARFs changed little neither. Qualitatively, there was a strong correlation between the PM levels and ARFs. In this section, through a detailed contrastive analysis, we examined the potential reasons for the occurrence of the two different patterns of haze pollution. We found that the crucial point in determining whether the PM mass concentration remained high or sharply decreased was related to whether the boundary layer remained stable. The boundary layer stability was, in turn notably linked to the PM mass concentration and aerosol radiative effect.

3.3 Quantitative analysis of the effect of particulate matter on the boundary layer structure

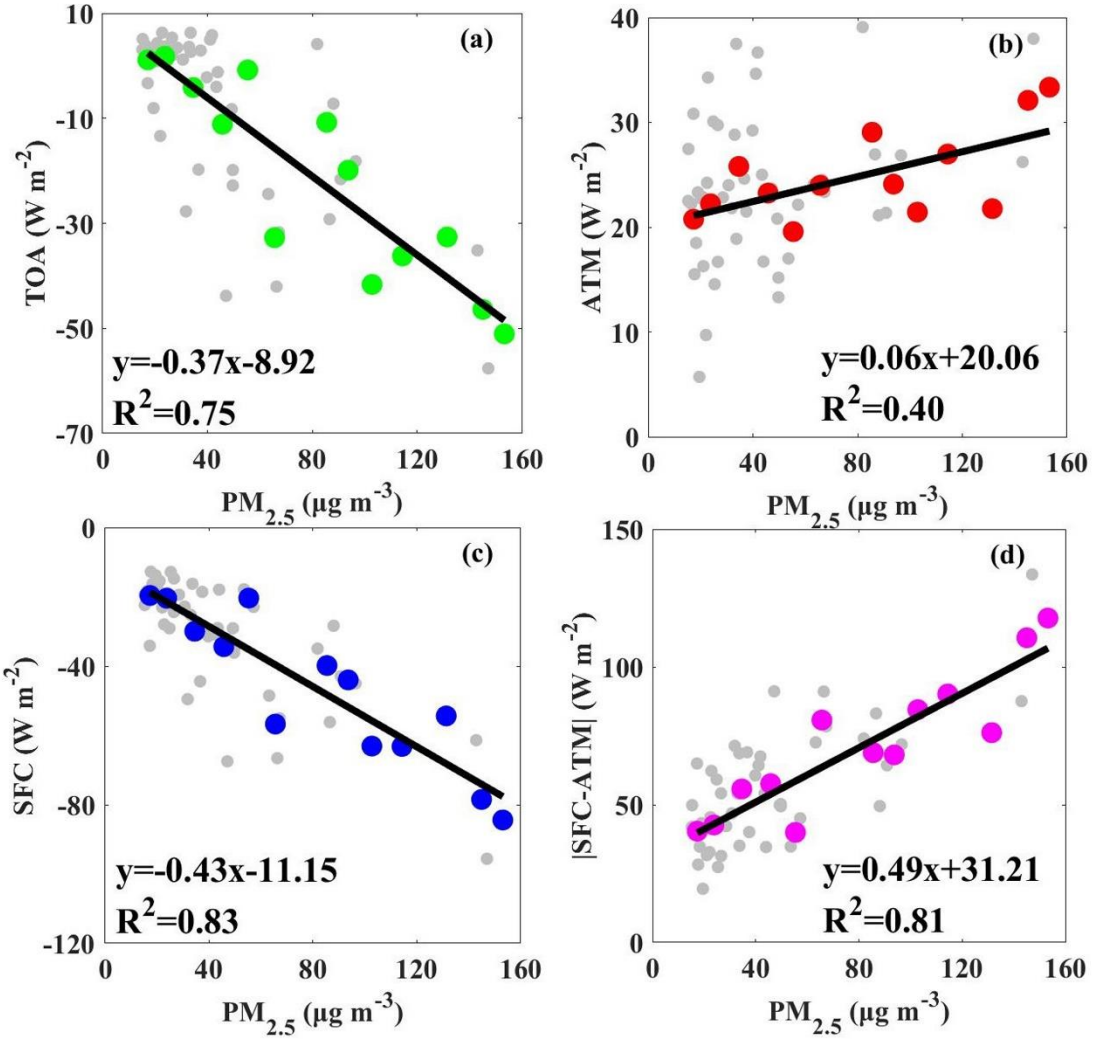

Figure 4. Scatter plots of the $PM_{2.5}$ mass concentration (x) versus aerosol radiative forcing at the surface (SFC; y; a), the interior of the atmospheric column (ATM; y; b), and top of the atmospheric column (TOA; y; c) as well as the absolute difference of SFC and ATM (|SFC-ATM|; y; d), respectively (gray dots: daily data; other dots: mean data). (The daily data means daily mean values of TOA, ATM, SFC, and corresponding daily averaged $PM_{2.5}$ mass concentration from 27 November 2018 to 25 January 2019 in Beijing. The mean $PM_{2.5}$ concentrations were obtained by averaging daily $PM_{2.5}$ concentrations at intervals of 10 μg m^{-3}. The mean TOA, ATM, and SFC were obtained after the corresponding daily TOA, ATM, and SFC average, respectively. For example, all daily $PM_{2.5}$ concentrations greater than 40 μg m^{-3} and less than 50 μg m^{-3} were

averaged as a mean $PM_{2.5}$ concentration, and TOA values (ATM; SFC) corresponding to this daily $PM_{2.5}$ concentration range were also averaged as a mean TOA (ATM; SFC)).

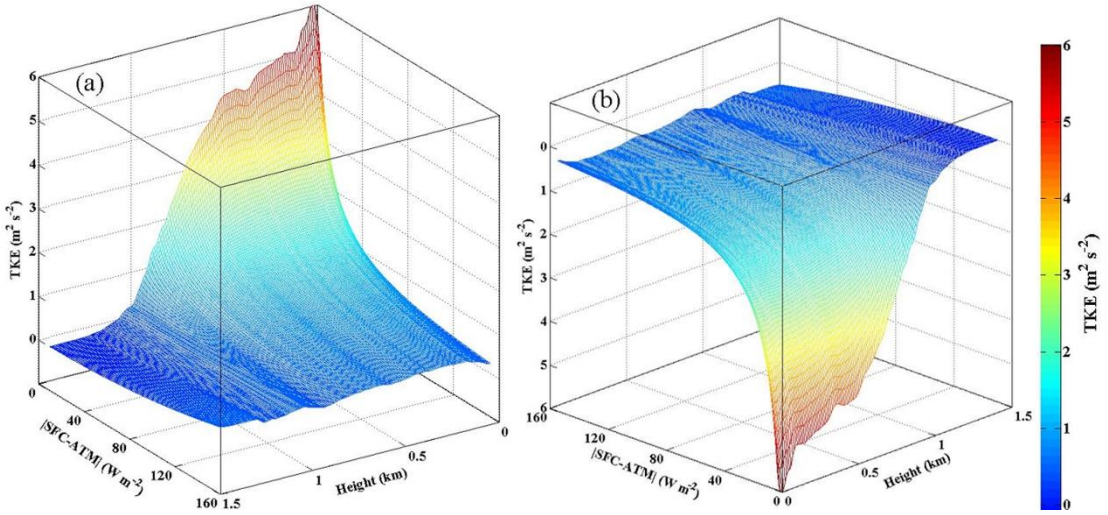

Figure 5. 3-D plot of the fitting relationship of the absolute difference in aerosol radiative forcing between the surface and interior of the atmospheric column (|SFC-ATM|; x) and turbulence kinetic energy (TKE; z) at the different altitudes (y) ((a) and (b) present different perspectives).

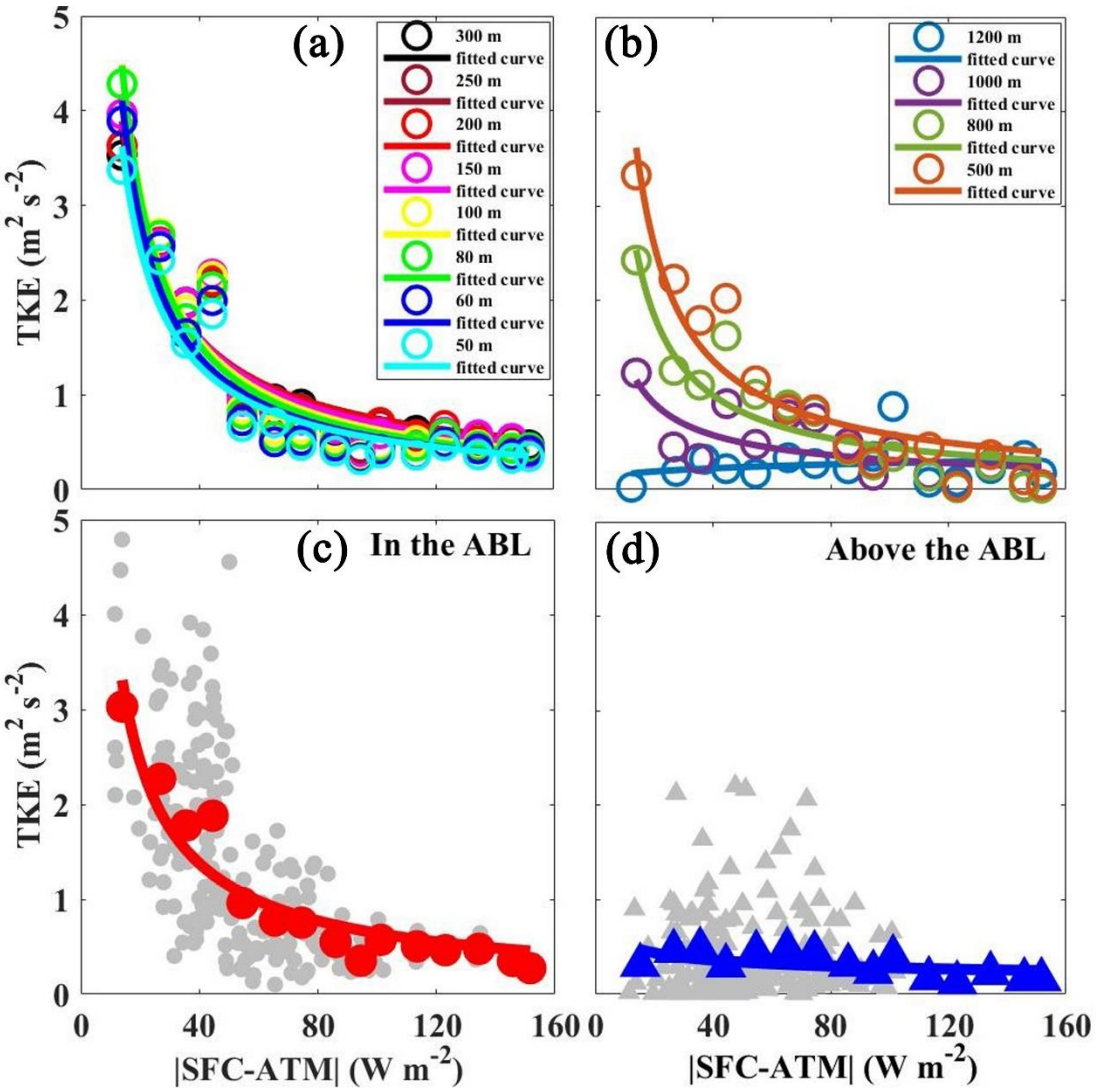

Figure 6. Scatter plots of the mean absolute difference of the aerosol radiative forcing at the surface and interior of the atmospheric column (|SFC-ATM|; x) versus the mean turbulence kinetic energy (TKE; y) at the different altitudes (a; b). Scatter plots of |SFC-ATM| (x) versus TKE (y) in the ABL (c) and above the ABL (d) (gray dots: hourly data; other dots: mean data). The hourly data were collected over a two-month period in Beijing from 27 November 2018 to 25 January 2019. (The hourly data means hourly mean values of |SFC-ATM| and corresponding hourly TKE. The mean |SFC-ATM| was obtained by averaging hourly |SFC-ATM| at intervals of 10 W m^{-2}, then the mean TKE was obtained after the average of the corresponding hourly TKE.).

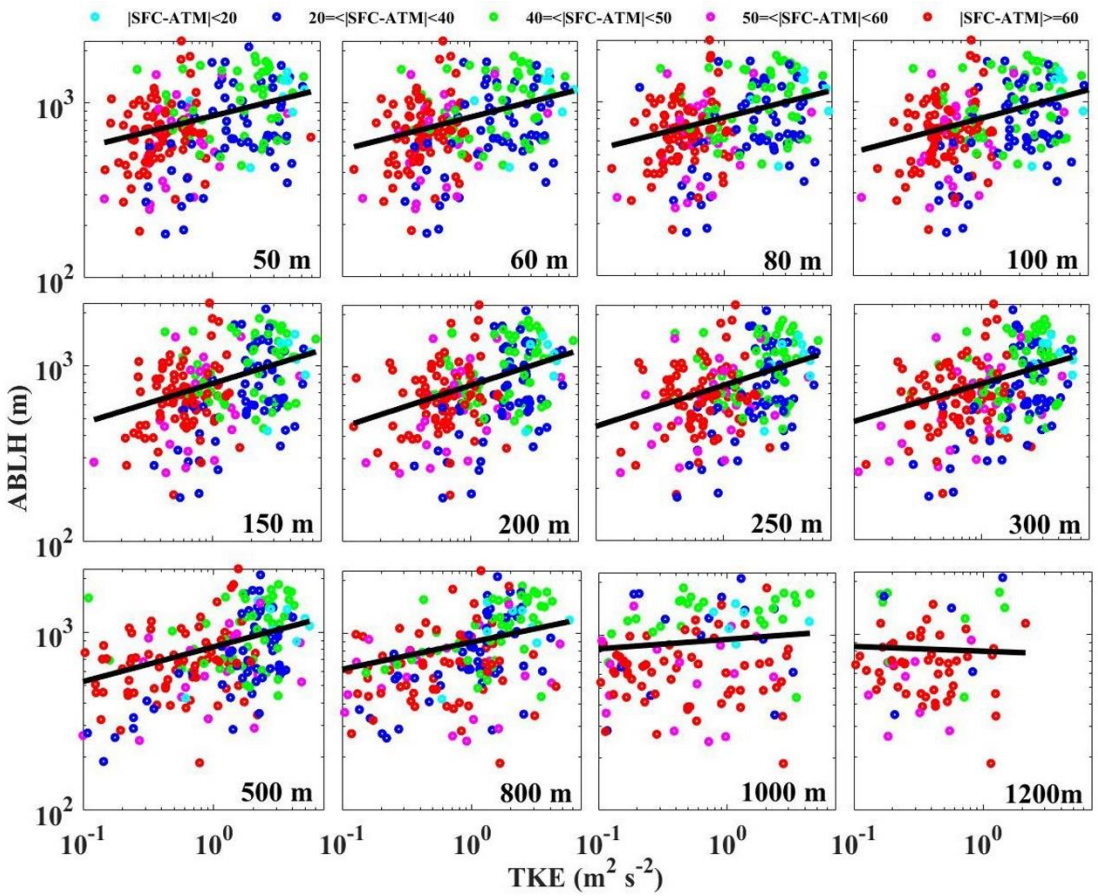

Figure 7. The atmospheric boundary layer height (ABLH; y) as a function of the turbulence kinetic energy (TKE; x) at the different altitudes and the aerosol radiative effect defined as |SFC-ATM| (color code). The calculated hourly data used above are collected over two months in Beijing from 27 November 2018 to 25 January 2019.

Based on the contrastive analysis in the previous section, it was clear that the stable ABL structure played a critical role in the outbreak and maintenance of air pollution. It appeared that the increase in atmospheric stability suppressed pollution diffusion under a weak turbulence activity and low ABLH. Water vapor also significantly accumulated to a relatively high level near the surface, further facilitating secondary aerosols' formation. The evolution of ABL stability essentially occurred in response to the atmospheric temperature structure, as analyzed above, which was influenced by the strong aerosol radiation effect (Li et al., 2010; Andrews, 2000). The Archimedes buoyancy generated by the pulsating temperature field in the gravity field exerted negative work on the turbulent pulsating field with a stable ABL occurring. The turbulence served as a carrier for substance transport in the boundary layer, such as

water vapor, heat, and PM. (Garratt et al., 1992). Generally, the ABL structure controlling pollutant dissipation, therefore dramatically relies on the turbulent activity. Thus, in the following section, the ARF and TKE were chosen as the key parameters to examine how PM affects and modifies the boundary layer structure.

Figure 4 shows the relationship between the PM concentration and ARF. The aerosol scattering effect results in less radiation reaching the ground and the top of the atmospheric column, so the solar radiation levels reaching the ground and at the top of the atmospheric column differ with or without ambient aerosols, thus making SFC and TOA forcing. As shown in Figs. 4(a) and (c), SFC and TOA, respectively, were proportional to the $PM_{2.5}$ concentration. With the increase in $PM_{2.5}$ concentration, elevated aerosol loading near the surface would scatter more solar radiation back into outer space and cause less solar radiation reaching the ground, corresponding to a cooling of the surface and making negative SFC. TOA means the aerosol radiative forcing at the top of the atmosphere column and is the sum of ATM and SFC. Considering that anthropogenic aerosols are mostly scattering aerosols, the SFC forcing is generally stronger than ATM, corresponding to a cooling of the earth-atmosphere system. The TOA forcing was thus usually negative and had a similar trend with SFC. ATM, driven by aerosol absorption and representing a warming effect of aerosols on the atmosphere layer, exhibited a positive correlation with the $PM_{2.5}$ concentration (see Fig. 4(b)). These results demonstrated that a higher $PM_{2.5}$ concentration would arouse a stronger ARF, further inhibiting solar radiation from reaching the ground, thus heating the atmosphere layer more. |SFC-ATM|, defined as the absolute value of the difference between SFC and ATM, represents aerosols' combined action on the solar radiation reaching the aerosol layer and the ground. Larger values of |SFC-ATM| indicate stronger aerosol scattering and/or absorption effects, further implying a more significant temperature difference between the ground and the above atmosphere layer. As expected, a positive linear correlation between |SFC-ATM| and $PM_{2.5}$ concentration was found, as shown in Fig. 4(d).

As described in the above paragraph, there was a strong ARF under a high PM loading, which markedly altered the atmospheric temperature structure, further

changing the ABL structure. It is necessary to determine the effect degree of ARF on the boundary layer structure. Figure 5 shows the 3-D plots of the fitting relationship between the hourly values of |SFC-ATM| and TKE at the different altitudes from different perspectives. What stood out in Fig. 5(a) was the general decline in TKE concerning the growth of |SFC-ATM|. With increasing |SFC-ATM| value, the TKE value at the different altitudes always decreased exponentially and approached zero below ~0.8 km. The notable exponential function between TKE and |SFC-ATM| explained that a strong ARF would drastically change the boundary layer into highly stable conditions characterized by a rather low TKE. The results above highlight the aerosol radiative effect's nonnegligible impact on the boundary layer structure, especially during the haze episode under a high aerosol loading with a strong ARF. It is well known that a larger net negative/positive SFC/ATM means a cooler/warmer the ground/atmosphere would be. An increase in |SFC-ATM| implies the gradual intensification of the ground cooling and/or atmosphere heating processes. Therefore, it changed the atmospheric stratification into a gradually enhanced stable state, which was characterized by increasingly weaker turbulence activities. Additionally, as shown in Fig. 5(b), we can identify a critical point of the |SFC-ATM| effects on TKE in the low layers from another perspective. In particular, TKE decreased with increasing |SFC-ATM| and hardly changed when |SFC-ATM| exceeded the critical point. To define the critical point, we generated scatter plots of the average |SFC-ATM| and TKE at several altitudes, as shown in Figs. 6(a)-(b). The scatter plots of the unaveraged hourly data are shown in Fig. S3, and the fitting functions are listed in Table S1. Depending on the exponential curve's maximum curvature (Silvanus and Gardner, 1998), a critical point should exist. With the mean TKE and |SFC-ATM| values on the exponential curve, we found that once the aerosol radiative effect defined by |SFC-ATM| exceeded 50-60 W m^{-2} (average of ~55 W m^{-2}), the TKE sharply decreased from ~2 m^2 s^{-2} to lower than 1 m^2 s^{-2}. This means that a high aerosol loading with a |SFC-ATM| value higher than ~55 W m^{-2} would change the boundary layer from the unstable state to the extremely stable state in a short time, and further increasing |SFC-ATM| would barely modify the ABL structure. This result can provide useful information to explain why air pollution

is sometimes aggravated under a stable ABL and sometimes not. The average aerosol radiative forcing (|SFC-ATM|) value of ~55 W m^{-2} can be defined as the threshold of the ARF effects on the ABL structure, which could provide useful information relevant model simulations, atmospheric environment improvement measures, and relevant policies. Besides, as shown in Figs. 5 and 6, the exponential relationship between TKE and |SFC-ATM| was notable in the low layers and gradually deteriorated with increasing altitude. On average, the exponential relationship was notable in the ABL and almost disappeared above the ABL (Figs. 6(c) and (d)). Considering that aerosols are mainly concentrated below the lower atmosphere, contributing the most to the SFC and ATM forcing, which further confirmed, the considerable change in atmospheric stratification caused by aerosols existed and mainly occurred in the lower layers.

The previous discussion shows that a strong aerosol radiative effect markedly affected the turbulent activity and modified the boundary layer structure. As many studies have reported, the ABLH is an important meteorological factor that influences the vertical diffusion of atmospheric pollutants and water vapor (Stull, 1988; Robert and Aron, 1983). The following examines the relationship among the turbulent activity, ARF, and ABLH to illustrate the change in ABLH in response to ARF. Figure 7 shows the ABLH as a function of the TKE and |SFC-ATM| at the different altitudes. It was apparent from this figure that a positive correlation exists between TKE and ABLH. As the turbulent activity became increasingly weaker, the corresponding boundary layer height gradually decreased, responding to the gradual increase in |SFC-ATM|. Similar to the relationship between the turbulent activity and aerosol radiative effect, as shown in Fig. 6, the relationship among these aspects was much stronger below 300 m and almost disappeared above 800 m. This further addressed the fact that the change in boundary layer height was attributed to the turbulence activity variation stemming from the aerosol radiative effect.

Thus far, this section has demonstrated that the aerosol loading with aerosol radiative effects impacted the turbulent activity, changed the boundary layer height, and modified the boundary layer structure. On the other hand, it is now necessary to explain how the renewed boundary layer structure modifies the $PM_{2.5}$ concentration. As shown

in Figs. S4(a)-(b), the ABLH as an independent variable impact the ambient water vapor in the ABL to some degree. There was a steady increase in the ambient humidity with decreasing ABLH, where absolute humidity (AH) and relative humidity (RH) were projected to decrease to ~3 g m^{-3} and ~60%, respectively, with the ABLH decreasing below ~500 m. With the increase in ambient humidity, a marked rise in $PM_{2.5}$ concentration occurred, as shown in Figs. S4(c)-(d). Once AH and RH exceeded ~3 g m^{-3} and ~60%, respectively, the $PM_{2.5}$ concentration reached ~100 μg m^{-3}. The results above indicate that with a fairly low boundary layer height, water vapor accumulated near the surface, and particles tended to hygroscopic grow, resulting in secondary aerosol formation in a high-humidity environment, further increasing the $PM_{2.5}$ concentration. As shown in Fig. S4(e), with the level off of the ABLH, the $PM_{2.5}$ mass concentration increased exponentially and reached a high value. The exponential relationship was similar to that between the ambient humidity and ABLH, which revealed that the explosive growth of the $PM_{2.5}$ concentration under a low ABLH was largely driven by intense secondary aerosol formation and hygroscopic growth at high ambient humidity.

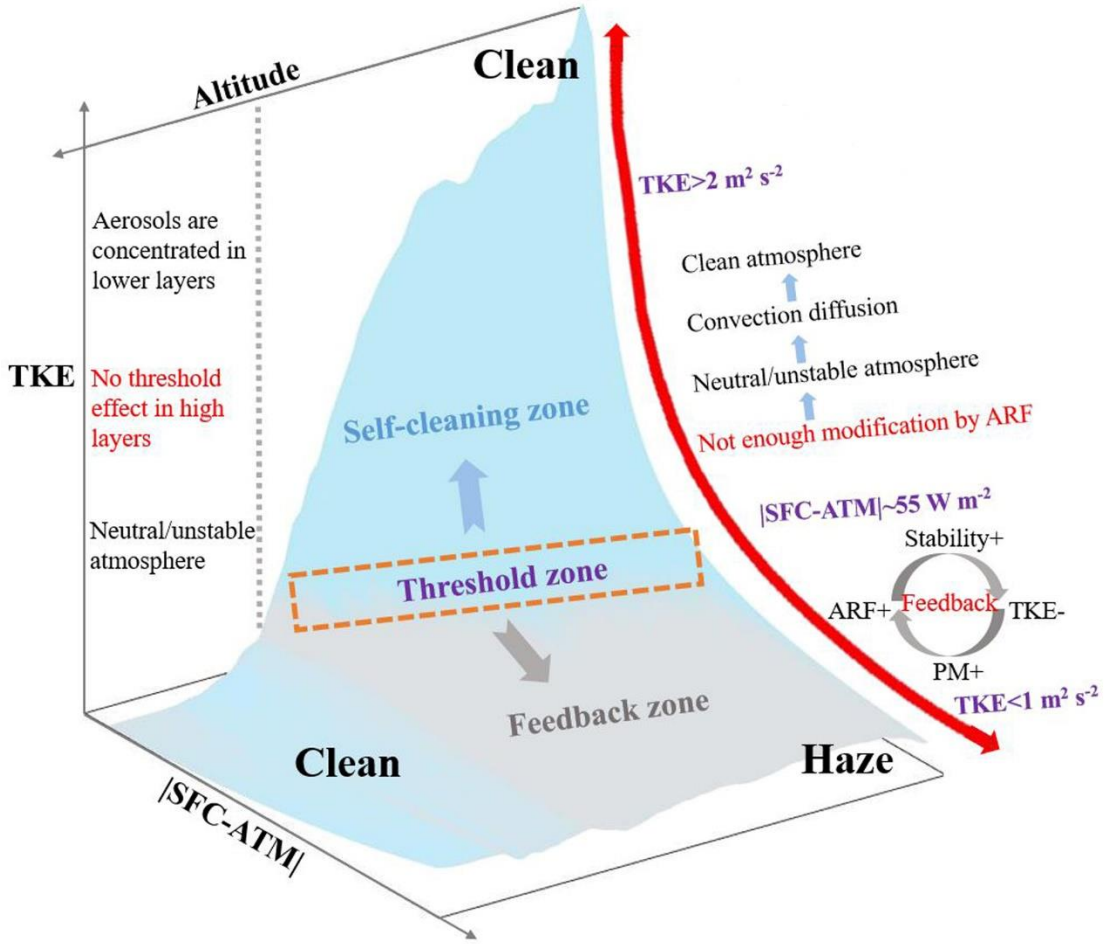

Figure 8. Schematic diagram of the interaction between the aerosol radiation forcing (ARF) and boundary layer structure (|SFC-ATM|: the mean absolute difference of the aerosol radiative forcing at the surface and interior of the atmospheric column; TKE: the mean turbulence kinetic energy).

4 Conclusion

By analyzing the two-month haze conditions in Beijing in winter, we found that haze pollution underwent two different variation patterns, namely, the same trends on the first two days, and on the next days, one haze pattern went through a continuing outbreak, while the other haze pattern exhibited notable diffusion. Considering equivalent emissions, this has raised important questions about whether and how the local boundary layer structure impacted/caused this difference. The results of a contrastive analysis qualitatively showed that the crucial point in determining whether the PM concentration remained very high or sharply decreased was related to whether the boundary layer structure (i.e., stability and TKE) satisfied relevant conditions. As

previous studies reported (Liu et al., 2018; Zhong et al., 2018b; Zhong et al., 2019) and was confirmed in this paper, the extremely stable stratification with positive $\partial\theta_{se}/\partial z$ values and a low TKE was the premise of the outbreak of haze pollution. The change/state of the boundary layer structure was, in turn, strongly linked to the PM mass concentration and ARF, and we further quantitatively evaluated the effect of ARF on the boundary layer structure. Figure 8, emerging from the previous observation analysis, is where ARF modifies the boundary layer structure and aggravates haze pollution. The ARF effects on the atmospheric stratification depend on the reduced radiation reaching the ground due to aerosol scattering and absorbing radiation in the atmosphere (Dickerson et al., 1997; Stone et al., 2008). First, we found that a positive linear relationship between |SFC-ATM| and $PM_{2.5}$ concentration existed, which means the strong aerosol scattering and/or absorption effect occurs during the heavy haze episodes and could arouse significant temperature differences between the surface and the above atmosphere layer. Secondly, previous studies revealed that black carbon solar absorption suppresses turbulence near the surface (Wilcox et al., 2016); however, we found that the TKE value at the different altitudes always decreased exponentially with increasing |SFC-ATM|, which was significant in the lower atmosphere layer. Moreover, the ARF effects on turbulent activity were found significant in the boundary layer and disappeared above the boundary layer, which also confirmed that the stronger ARF from the aerosol layer would indeed change the boundary layer into the considerably stable state characterized by a relatively low TKE. Then, the ARF change is linear due to the PM concentration; however, the influence of ARF on the boundary layer structure is nonlinear. Based on the exponential relationship, the threshold of the ARF effects on the boundary layer structure has been determined for the first time in this paper, highlighting that once the ARF exceeded a specific value, the boundary layer structure would quickly stabilize after that changed little with increasing ARF. This threshold can provide useful information for relevant atmospheric environment improvement measures and policies. When the $PM_{2.5}$ concentration is controlled with the ARF below the threshold, the unstable atmosphere's self-purification capacity can effectively dilute and diffuse pollutants. In contrast, when the $PM_{2.5}$ concentration increases with an ARF

exceeding the threshold value, the boundary layer stabilizes sharply, especially in the lower layers, aggravating haze pollution.

Data availability

The surface $PM_{2.5}$ & PM_{10} and other trace gases observation data used in this study can be accessed from http://106.37.208.233:20035/ (last access: 4 June 2020). Other datasets can be accessed upon request to the corresponding author.

Author contribution

ZD performed the research and wrote the paper. XJ provided writing guidance, revised and polished the paper. GC performed the SBDART model. QJ and WY GC contributed to discussions of results. TG and MY designed the experiments, and DL, WX, LG, and MY carried them out. All the authors have made substantial contributions to the work reported in the manuscript.

Competing interests

The authors declare that they have no conflict of interest.

Acknowledgments

This study was supported by the Ministry of Science and Technology of China (grant number 2016YFC0202001), the CAS Strategic Priority Research Program (XDA23020301), and the National Natural Science Foundation of China (grant number 41375036). The authors are thankful for the data support from the National Earth System Science Data Sharing Infrastructure, National Science and Technology Infrastructure of China (available at http://www.geodata.cn, last access: 4 June 2020).

References

An, Z., Huang, R.-J., Zhang, R., Tie, X., Li, G., Cao, J., Zhou, W., Shi, Z., Han, Y., Gu, Z., and Ji, Y.: Severe haze in northern China: A synergy of anthropogenic emissions and atmospheric processes, Proc. Natl. Acad. Sci. U. S. A., 116, 8657-8666, https://doi.org/10.1073/pnas.1900125116, 2019.

Andrews, D. G.: An Introduction to Atmospheric Physics, Cambridge University Press, 2000.

Banta, R. M., Pichugina, Y. L., and Brewer, W. A.: Turbulent velocity-variance profiles in the stable boundary layer generated by a nocturnal low-level jet, J. Atmos. Sci., 63, 2700-2719, https://doi.org/10.1175/jas3776.1, 2006.

Barbaro, E., Arellano, J., Ouwersloot, H., Schröter, J., Donovan, D., and Krol, M.: Aerosols in the

convective boundary layer: Shortwave radiation effects on the coupled land-atmosphere system, J. Geophys. Res.: Atmos., 119, 5845–5863, https://doi.org/10.1002/2013JD021237, 2014.

Dickerson, R. R., Kondragunta, S., Stenchikov, G., Civerolo, K. L., Doddridge, B. G., and Holben, B. N.: The impact of aerosols on solar ultraviolet radiation and photochemical smog, Science (New York, N.Y.), 278, 827-830, https://doi.org/10.1126/science.278.5339.827, 1997.

Garratt, J. R., Dessler, A. J., Houghton, J. T., and Rycroft, M. J.: The atmospheric boundary layer, 1992.

Ding, A., Huang, X., Nie, W., Sun, J., Kerminen, V.-M., Petäjä, T., Su, H., Cheng, Y., Yang, X., Wang, M., Chi, X., Wang, J., Virkkula, A., Guo, W., Yuan, J., Wang, S., Zhang, R., Wu, Y., Song, Y., Zhu, T., Zilitinkevich, S., and Kulmala, M.: Enhanced haze pollution by black carbon in megacities in China, Geophys. Res. Lett., 43, 2873–2879, https://doi.org/10.1002/2016GL067745, 2016.

Gong, C., Xin, J., Wang, S., Wang, Y., Wang, P., Wang, L., and Li, P.: The aerosol direct radiative forcing over the Beijing metropolitan area from 2004 to 2011, J. Aerosol Sci., 69, 62-70, https://doi.org/10.1016/j.jaerosci.2013.12.007, 2014.

Gregory, L.: Cimel Sunphotometer (CSPHOT) Handbook, 2011.

Guo, S., Hu, M., Zamora, M. L., Peng, J., Shang, D., Zheng, J., Du, Z., Wu, Z., Shao, M., Zeng, L., Molina, M. J., and Zhang, R.: Elucidating severe urban haze formation in China, Proc. Natl. Acad. Sci. U. S. A., 111, 17373-17378, https://doi.org/10.1073/pnas.1419604111, 2014.

Haman, C. L., Couzo, E., Flynn, J. H., Vizuete, W., Heffron, B., and Lefer, B. L.: Relationship between boundary layer heights and growth rates with ground-level ozone in Houston, Texas, J. Geophys. Res.: Atmos., 119, 6230-6245, https://doi.org/10.1002/2013jd020473, 2014.

Han, S., Bian, H., Tie, X., Xie, Y., Sun, M., and Liu, A.: Impact of nocturnal planetary boundary layer on urban air pollutants: Measurements from a 250-m tower over Tianjin, China, J. Hazard. Mater., 162, 264-269, https://doi.org/10.1016/j.jhazmat.2008.05.056, 2009.

Hua, Y., Wang, S., Wang, J., Jiang, J., Zhang, T., Song, Y., Kang, L., Zhou, W., Cai, R., Wu, D., Fan, S., Wang, T., Tang, X., Wei, Q., Sun, F., and Xiao, Z.: Investigating the impact of regional transport on PM2.5 formation using vertical observation during APEC 2014 Summit in Beijing, Atmos. Chem. Phys., 16, 15451-15460, https://doi.org/10.5194/acp-16-15451-2016, 2016.

Huang, X., Wang, Z., and Ding, A.: Impact of Aerosol-PBL Interaction on Haze Pollution: Multiyear Observational Evidences in North China, Geophys. Res. Lett., 45, 8596-8603,

https://doi.org/10.1029/2018gl079239, 2018.

Jin-Xiang, L. I.: The Characteristics and Cause Analysis of Heavy-Air-Pollution in Autumn and Winter in Beijing, Environ. Monit. China, 2007.

Kotthaus, S., and Grimmond, C. S. B.: Atmospheric boundary-layer characteristics from ceilometer measurements. Part 1: A new method to track mixed layer height and classify clouds, Q. J. R. Meteorol. Soc., 144, 1525-1538, https://doi.org/10.1002/qj.3299, 2018.

Lee K., Li Z., Wong M., Xin J., Wang Y., Hao W., and Zhao F.: Aerosol single scattering albedo estimated across China from a combination of ground and satellite measurements, J. Geophys. Res.: Atmos., 112(D22), https://doi.org/10.1029/2007JD009077, 2007.

Levy, R. C., Remer, L. A., and Dubovik, O.: Global aerosol optical properties and application to Moderate Resolution Imaging Spectroradiometer aerosol retrieval over land, J. Geophys. Res.: Atmos., 112, https://doi.org/10.1029/2006jd007815, 2007.

Li, G., Bei, N., Cao, J., Huang, R., Wu, J., Feng, T., Wang, Y., Liu, S., Zhang, Q., Tie, X., and Molina, L. T.: A possible pathway for rapid growth of sulfate during haze days in China, Atmos. Chem. Phys., 17, 3301-3316, https://doi.org/10.5194/acp-17-3301-2017, 2017.

Li, M., Wang, L., Liu, J., Gao, W., Song, T., Sun, Y., Li, L., Li, X., Wang, Y., Liu, L., Daellenbach, K. R., Paasonen, P. J., Kerminen, V.-M., Kulmala, M., and Wang, Y.: Exploring the regional pollution characteristics and meteorological formation mechanism of PM2.5 in North China during 2013-2017, Environ. Int., 134, https://doi.org/10.1016/j.envint.2019.105283, 2020.

Li, Z., Lee, K.-H., Wang, Y., Xin, J., and Hao, W.-M.: First observation-based estimates of cloud-free aerosol radiative forcing across China, J. Geophys. Res.: Atmos., 115, https://doi.org/10.1029/2009jd013306, 2010.

Liu, Q., Jia, X., Quan, J., Li, J., Li, X., Wu, Y., Chen, D., Wang, Z., and Liu, Y.: New positive feedback mechanism between boundary layer meteorology and secondary aerosol formation during severe haze events, Sci Rep, 8, https://doi.org/10.1038/s41598-018-24366-3, 2018.

Liu, T. T., Gong, S., Meng, Y., Qi, C. Z., and Hong, L. L.: Contributions of meteorology and emission to the 2015 winter severe haze pollution episodes in Northern China, Atmos. Chem. Phys., 17, 1-17, https://doi.org/10.5194/acp-2016-204, 2016.

Münkel, C., Eresmaa, N., Rasanen, J., and Karppinen, A.: Retrieval of mixing height and dust concentration with lidar ceilometer, Bound-Lay Meteorol, 124, 117-128, https://doi.org/

10.1007/s10546-006-9103-3, 2007.

Ma, Q., Wu, Y., Zhang, D., Wang, X., and Zhang, R.: Roles of regional transport and heterogeneous reactions in the PM 2.5 increase during winter haze episodes in Beijing, Sci. Total Environ., 599-600, 246-253, https://doi.org/10.1016/j.scitotenv.2017.04.193, 2017.

Miao, Y., Guo, J., Liu, S., Zhao, C., Li, X., Zhang, G., Wei, W., and Ma, Y.: Impacts of synoptic condition and planetary boundary layer structure on the trans-boundary aerosol transport from Beijing-Tianjin-Hebei region to northeast China, Atmos. Environ., 181, 1-11, https://doi.org/10.1016/j.atmosenv.2018.03.005, 2018.

Munro, D. S.: Boundary Layer Climatology, 2005.

Niu, F., Li, Z., Li, C., Lee, K.-H., and Wang, M.: Increase of wintertime fog in China: Potential impacts of weakening of the Eastern Asian monsoon circulation and increasing aerosol loading, J. Geophys. Res.: Atmos., 115, https://doi.org/10.1029/2009jd013484, 2010.

Petaja, T., Jarvi, L., Kerminen, V. M., Ding, A. J., Sun, J. N., Nie, W., Kujansuu, J., Virkkula, A., Yang, X. Q., Fu, C. B., Zilitinkevich, S., and Kulmala, M.: Enhanced air pollution via aerosol-boundary layer feedback in China, Sci Rep, 6, https://doi.org/10.1038/srep18998, 2016.

Pichugina, Y. L., Banta, R. M., Bonin, T., Brewer, W. A., Choukulkar, A., McCarty, B. J., Baidar, S., Draxl, C., Fernando, H. J. S., Kenyon, J., Krishnamurthy, R., Marquis, M., Olson, J., Sharp, J., and Stoelinga, M.: Spatial Variability of Winds and HRRR-NCEP Model Error Statistics at Three Doppler-Lidar Sites in the Wind-Energy Generation Region of the Columbia River Basin, J. Appl. Meteorol. Climatol., 58, 1633-1656, https://doi.org/10.1175/jamc-d-18-0244.1, 2019.

Quan, J., Gao, Y., Zhang, Q., Tie, X., Cao, J., Han, S., Meng, J., Chen, P., and Zhao, D.: Evolution of planetary boundary layer under different weather conditions, and its impact on aerosol concentrations, Particuology, 11, 34-40, https://doi.org/10.1016/j.partic.2012.04.005, 2013.

Robert, and Aron: Mixing height—an inconsistent indicator of potential air pollution concentrations, Atmos. Environ., 17, 2193-2197, https://doi.org/10.1016/0004-6981(83)90215-9, 1983.

Schaefer, K., Wang, Y., Muenkel, C., Emeis, S., Xin, J., Tang, G., Norra, S., Schleicher, N., Vogt, J., and Suppan, P.: Evaluation of continuous ceilometer-based mixing layer heights and correlations with PM2.5 concentrations in Beijing, in: Remote Sensing of Clouds and the Atmosphere Xiv, edited by: Picard, R. H., Schafer, K., Comeron, A., Kassianov, E., and Mertens, C. J., Proceedings of SPIE, 2009.

Silvanus, P. T. F. R. S., and Gardner, M.: A Little More about Curvature of Curves, Calculus Made Easy, 249-262, https://doi.org/10.1007/978-1-349-15058-8_25, 1998.

Stone, R. S., Anderson, G. P., Shettle, E. P., Andrews, E., Loukachine, K., Dutton, E. G., Schaaf, C., and Roman, M. O., III: Radiative impact of boreal smoke in the Arctic: Observed and modeled, J. Geophys. Res.: Atmos., 113, https://doi.org/10.1029/2007jd009657, 2008.

Stull, R. B.: An Introduction to Boundary Layer Meteorology, 1988.

Su, T., Li, Z., and Kahn, R.: Relationships between the planetary boundary layer height and surface pollutants derived from lidar observations over China: regional pattern and influencing factors, Atmos. Chem. Phys., 18, 15921-15935, https://doi.org/10.5194/acp-18-15921-2018, 2018.

Tang, G., Zhu, X., Hu, B., Xin, J., Wang, L., Münkel, C., Mao, G., and Wang, Y.: Impact of emission controls on air quality in Beijing during APEC 2014: lidar ceilometer observations, Atmos. Chem. Phys., 15, 12667–12680, https://doi.org/10.5194/acp-15-12667-2015, 2015.

Tang, G., Zhang, J., Zhu, X., Song, T., Muenkel, C., Hu, B., Schaefer, K., Liu, Z., Zhang, J., Wang, L., Xin, J., Suppan, P., and Wang, Y.: Mixing layer height and its implications for air pollution over Beijing, China, Atmos. Chem. Phys., 16, 2459-2475, https://doi.org/10.5194/acp-16-2459-2016, 2016.

Tie, X., Huang, R.-J., Cao, J., Zhang, Q., Cheng, Y., Su, H., Chang, D., Poeschl, U., Hoffmann, T., Dusek, U., Li, G., Worsnop, D. R., and O'Dowd, C. D.: Severe Pollution in China Amplified by Atmospheric Moisture, Sci Rep, 7, https://doi.org/10.1038/s41598-017-15909-1, 2017.

Wang, J. Z., Gong, S. L., Zhang, X. Y., Yang, Y. Q., Hou, Q., Zhou, C. H., and Wang, Y. Q.: A Parameterized Method for Air-Quality Diagnosis and Its Applications, Adv. Meteorol., https://doi.org/10.1155/2012/238589, 2012.

Wang, L., Liu, J., Gao, Z., Li, Y., Huang, M., Fan, S., Zhang, X., Yang, Y., Miao, S., Zou, H., Sun, Y., Chen, Y., and Yang, T.: Vertical observations of the atmospheric boundary layer structure over Beijing urban area during air pollution episodes, Atmos. Chem. Phys., 19, 6949-6967, https://doi.org/10.5194/acp-19-6949-2019, 2019.

Wang, X., Wei, W., Cheng, S., Li, J., Zhang, H., and Lv, Z.: Characteristics and classification of PM 2.5 pollution episodes in Beijing from 2013 to 2015, Sci. Total Environ., 612, 170-179, https://doi.org/10.1016/j.scitotenv.2017.08.206, 2018.

Wang, Y., Yao, L., Wang, L., Liu, Z., Ji, D., Tang, G., Zhang, J., Sun, Y., Hu, B., and Xin, J.:

Mechanism for the formation of the January 2013 heavy haze pollution episode over central and eastern China, Sci. China-Earth Sci., 57, 14-25, https://doi.org/10.1007/s11430-013-4773-4, 2014.

Wilcox, E. M., Thomas, R. M., Praveen, P. S., Pistone, K., Bender, F. A. M., and Ramanathan, V.: Black carbon solar absorption suppresses turbulence in the atmospheric boundary layer, Proc. Natl. Acad. Sci. U. S. A., 113, 11794-11799, https://doi.org/10.1073/pnas.1525746113, 2016.

Xin, J., Gong, C., Wang, S., and Wang, Y.: Aerosol direct radiative forcing in desert and semi-desert regions of northwestern China, Atmos. Res., 171, 56-65, https://doi.org/10.1016/j.atmosres.2015.12.004, 2016.

Xu, T., Song, Y., Liu, M., Cai, X., Zhang, H., Guo, J., and Zhu, T.: Temperature inversions in severe polluted days derived from radiosonde data in North China from 2011 to 2016, Sci. Total Environ., 647, 1011-1020, https://doi.org/10.1016/j.scitotenv.2018.08.088, 2019.

Yu, H., Liu, S., and Dickinson, R.: Radiative effects of aerosols on the evolution of the atmospheric boundary layer, J. Geophys. Res., 107(D12), 1, 4142–14, https://doi.org/10.1029/2001JD000754, 2002.

Yang, Y., Liao, H., and Lou, S.: Increase in winter haze over eastern China in recent decades: Roles of variations in meteorological parameters and anthropogenic emissions, J. Geophys. Res.: Atmos., 121, 13050-13065, https://doi.org/10.1002/2016jd025136, 2016.

Zhang, Q., Ma, Q., Zhao, B., Liu, X., Wang, Y., Jia, B., and Zhang, X.: Winter haze over North China Plain from 2009 to 2016: Influence of emission and meteorology, Environ. Pollut., 242, 1308-1318, https://doi.org/10.1016/j.envpol.2018.08.019, 2018.

Zhang, R., Khalizov, A. F., Pagels, J., Zhang, D., Xue, H., and McMurry, P. H.: Variability in morphology, hygroscopicity, and optical properties of soot aerosols during atmospheric processing, Proc. Natl. Acad. Sci. U. S. A., 105, 10291-10296, https://doi.org/10.1073/pnas.0804860105, 2008.

Zhang, Z., Zhang, X., Zhang, Y., Wang, Y., Zhou, H., Shen, X., Che, H., Sun, J., and Zhang, L.: Characteristics of chemical composition and role of meteorological factors during heavy aerosol pollution episodes in northern Beijing area in autumn and winter of 2015, Tellus Series B-Chemical and Physical Meteorology, 69, https://doi.org/10.1080/16000889.2017.1347484, 2017.

Zhao, D., Xin, J., Gong, C., Quan, J., Liu, G., Zhao, W., Wang, Y., Liu, Z., and Song, T.: The formation mechanism of air pollution episodes in Beijing city: Insights into the measured feedback between aerosol radiative forcing and the atmospheric boundary layer stability, Sci. Total Environ.,

692, 371-381, https://doi.org/10.1016/j.scitotenv.2019.07.255, 2019.

Zheng, C., Zhao, C., Zhu, Y., Wang, Y., Shi, X., Wu, X., Chen, T., Wu, F., and Qiu, Y.: Analysis of influential factors for the relationship between PM2.5 and AOD in Beijing, Atmos. Chem. Phys., 17, 13473-13489, https://doi.org/10.5194/acp-17-13473-2017, 2017.

Zheng, G. J., Duan, F. K., Su, H., Ma, Y. L., Cheng, Y., Zheng, B., Zhang, Q., Huang, T., Kimoto, T., Chang, D., Poeschl, U., Cheng, Y. F., and He, K. B.: Exploring the severe winter haze in Beijing: the impact of synoptic weather, regional transport and heterogeneous reactions, Atmos. Chem. Phys., 15, 2969-2983, https://doi.org/10.5194/acp-15-2969-2015, 2015.

Zhong, J., Zhang, X., Wang, Y., Sun, J., Zhang, Y., Wang, J., Tan, K., Shen, X., Che, H., Zhang, L., Zhang, Z., Qi, X., Zhao, H., Ren, S., and Li, Y.: Relative Contributions of Boundary-Layer Meteorological Factors to the Explosive Growth of PM2.5 during the Red-Alert Heavy Pollution Episodes in Beijing in December 2016, J. Meteorol. Res., 31, 809-819, https://doi.org/10.1007/s13351-017-7088-0, 2017.

Zhong, J., Zhang, X., Wang, Y., Liu, C., and Dong, Y.: Heavy aerosol pollution episodes in winter Beijing enhanced by radiative cooling effects of aerosols, Atmos. Res., 209, 59-64, https://doi.org/10.1016/j.atmosres.2018.03.011, 2018a.

Zhong, J., Zhang, X., Dong, Y., Wang, Y., Liu, C., Wang, J., Zhang, Y., and Che, H.: Feedback effects of boundary-layer meteorological factors on cumulative explosive growth of PM2.5 during winter heavy pollution episodes in Beijing from 2013 to 2016, Atmos. Chem. Phys., 18, 247–258, https://doi.org/10.5194/acp-18-247-2018, 2018b.

Zhong, J., Zhang, X., Wang, Y., Wang, J., Shen, X., Zhang, H., Wang, T., Xie, Z., Liu, C., Zhang, H., Zhao, T., Sun, J., Fan, S., Gao, Z., Li, Y., and Wang, L.: The two-way feedback mechanism between unfavorable meteorological conditions and cumulative aerosol pollution in various haze regions of China, Atmos. Chem. Phys., 19, 3287–3306, https://doi.org/10.5194/acp-19-3287-2019, 2019.

Zhu, X., Tang, G., Lv, F., Hu, B., Cheng, M., Muenkel, C., Schafer, K., Xin, J., An, X., Wang, G., Li, X., and Wang, Y.: The spatial representativeness of mixing layer height observations in the North China Plain, Atmos. Res., 209, 204-211, https://doi.org/10.1016/j.atmosres.2018.03.019, 2018.